Inorganic Chemistry

pubs.acs.org/IC Article

A Generalized Semiempirical Approach to the Modeling of the Optical Band Gap of Ternary Al-(Ga, Nb, Ta, W) Oxides Containing Different Alumina Polymorphs

Francesco Di Quarto,* Andrea Zaffora, Francesco Di Franco, and Monica Santamaria

Cite This: *Inorg. Chem.* 2021, 60, 1419−1435 Read Online

ACCESS | Metrics & More | Article Recommendations | Supporting Information

ABSTRACT: A generalization of the modeling equation of optical band gap values for ternary oxides, as a function of cationic ratio composition, is carried out based on the semiempirical correlation between the differences in the electronegativity of oxygen and the average cationic electronegativity proposed some years ago. In this work, a novel approach is suggested to account for the differences in the band gap values of the different polymorphs of binary oxides as well as for ternary oxides existing in different crystalline structures. A preliminary test on the validity of the proposed modeling equations has been carried out by using the numerous experimental data pertaining to alumina and gallia polymorphs as well as the crystalline ternary $Ga_{(1-x)}Al_xO_3$ polymorphs (α-$Ga_{(1-x)}Al_xO_3$ and β-$Ga_{(1-x)}Al_xO_3$) covering a large range of optical band gap values (4.50−8.50 eV). To make a more rigorous test of the modeling equation, we extended our investigation to amorphous ternary oxides anodically formed on Al-d-metal alloys (Al-Nb, Al-Ta, and Al-W) covering a large range of d-metal composition ($x_{\text{d-metal}} \geq 0.2$). In the last case, the novel approach allows one to overcome some difficulties experienced in fitting the optical band gap dependence from the Al-d-metal mixed anodic oxide composition as well as to provide a rationale for the departure, at the lowest d-metal content ($x_{\text{d-metal}} < 0.2$), from the behavior observed for anodic films containing higher d-metal content.

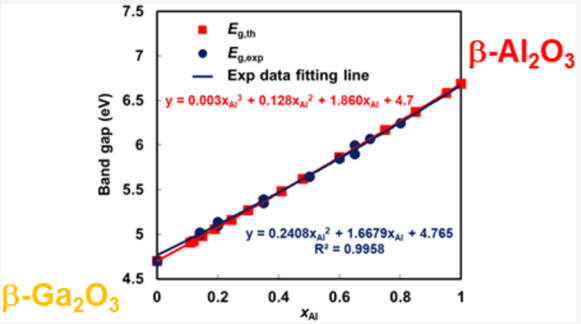

1. INTRODUCTION

Band gap modeling of simple and complex oxides is of paramount importance for the application of such materials in numerous and important applications pertaining to different fields such as solar energy conversion (photoelectrochemical and photovoltaic solar cells, photocatalysis, and electrocatalysis), microelectronics (high-*k*, high-band-gap materials and resistive random access memory (ReRAM)), and active and passive anticorrosive coatings.[1−7] Owing to this, the band structure calculation of solids and, notably, of oxides has been one of the most investigated subjects of materials science in the past 20 years or more.[8] In spite of the rewarding achievements obtained in computing numerous solid-state properties of different materials, the prediction of band gap values of materials is still a formidable task also for the most advanced quantum mechanical methods rooted on density functional theory (DFT).[1,8−15]

Apart from the theoretical difficulties and computing cost in predicting reliable band gap values for different materials, a further complication arises when a comparison of E_g values, obtained by using theoretical models, is carried out for an assigned material.[9,10] This task is made further complicated by the large variability of experimental band gap values reported in the literature for a given material. The variability in the experimental E_g values, not always accounted for the comparison, can originate from different sources pertaining to the different experimental techniques (electron energy loss spectroscopy (EELS), variable angle spectroscopy ellipsometry (VASE), diffuse reflectance spectroscopy (DRS), photocurrent spectroscopy (PCS), etc.) used to extract the E_g value as well as in the data treatment model employed in deriving the band gap values.[16−19] Moreover, the assumption of identical composition and structure should have to be carefully checked, especially in the presence of differences in the method of fabrication of the investigated material.

This aspect is particularly intriguing in the case of thin films of oxides obtained by using different growth techniques or grown in different conditions but with the same technique. In the case of anodic oxide films grown by anodizing in different solutions, two common sources of variability can be attributed to the differences in the crystallinity degree of the anodic films as well as to the possible incorporation, into the oxide film, of

Received: September 8, 2020
Published: January 20, 2021

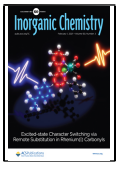

https://dx.doi.org/10.1021/acs.inorgchem.0c02691
Inorg. Chem. 2021, 60, 1419−1435

chemical species derived from reacting species lying in solution.[20−26]

In a previous work,[27] we have shown that it is possible to correlate semiempirically the optical band gap values of numerous crystalline binary oxides to their composition by means of a general expression as

$$E_g = A(\chi_O - \chi_M)^2 + B \quad (1)$$

where χ_M and χ_O are the electronegativities (ENs) of metal and oxygen, respectively, in Pauling's scale. A and B have been determined by a linear best fitting procedure of experimental E_g values vs $(\chi_O - \chi_M)^2$.

In the case of pure s,p and d-metal oxides, two different interpolating straight lines were derived with

$$A_{d-met} = 1.35 \quad B_{d-met} = -1.49\ [eV] \quad (2)$$

for d-metal oxides and

$$A_{s,p-met} = 2.17 \quad B_{s,p-met} = -2.71\ [eV] \quad (3)$$

for s,p-metal oxides. An analogous correlation has been shown to hold also for AlN, GaN, and InN compounds and their alloys.[28]

Equations 1 and 2 were able to fit, with a reasonable accuracy and with some discussed exceptions,[27] the E_g values of many f,d-metal oxides (III−XII groups and TM-oxides), while eqs 1 and 3 were able to reproduce with good accuracy the experimental E_g values of sp-metal oxides (II and XIII−XV groups in the periodic table of the elements).

More recently,[29−32] in an attempt to perform photocurrent spectroscopy (PCS), a more quantitative technique for the in situ characterization of surface passive films and corrosion layers grown on metallic alloys, we tried to extend the proposed correlations valid for pure binary oxides to regular (sp-sp; d-d) and nonregular (sp-d) ternary oxides. We are aware[32] that the most critical aspects of our semiempirical approach, especially when extended to multinary oxides, are related to the following:[32,33]

a The lack of any dependence of estimated E_g on the nature of optical transitions (direct or indirect) determining the optical band gap values.

b The limited ability of eq 1 in accounting for the different optical band gap values of different polymorphs by assuming for the electronegativity value, χ_M, of each cation metal an uncertainty range equal to ±0.05 around the χ_M^0 value reported in Pauling's scale[34] ($\chi_M = \chi_M^0 \pm 0.05$).

We have shown[29,30,32] that the semiempirical approach initially proposed for pure oxides is able to model the optical band gap behavior of more complex multinary oxides, as a function of their composition, once some further refinements to the initial approach are introduced, which account, at least partially, for the criticisms previously reported in the literature.[33]

In this paper, we will discuss how to extend the initial correlation to the case of different polymorphs by treating extensively some Al-based ternary oxides containing both sp- and d-metal cations. In particular, we will discuss some technically relevant systems like $Ga_xAl_{(1-x)}O_3$ ternary oxides, finding numerous applications as wide band gap materials in the field of high-power electronic devices and solar-blind ultraviolet (UV) photodetectors.[35−39] Al-Ga mixed oxides, moreover, are the basis for the fabrication of rare earth (RE)-aluminum garnet ($Y_3(Al_xGa_{1-x})_5O_{12}$ (YAGG), $Lu_3(Al_xGa_{1-x})_5O_{12}$ (LuAGG), and $Gd_3(Al_xGa_{1-x})_5O_{12}$ (GAGG)), which, doped with various trivalent RE-cations, are widely used as optical materials in technologically relevant applications including light-emitting diodes (LEDs), plasma display panels, and scintillator materials used in medical imaging techniques.[40−42]

As for the high-band-gap (>3 eV) ternary amorphous oxides, apart from their importance in the field of corrosion protection, the Al-d-metal amorphous mixed oxides are currently under investigation for their possible use in the field of electrical and electronic engineering as high-k materials in microelectronics[3,4] and in advanced electrolytic capacitors.[43] Ta-based ternary amorphous oxides, with high thermal stability and suitable refractive index, have been used and are under current investigation as high-resolution light mirrors in interferometric detectors, including those of recent gravitational waves in LIGO experiments.[44−48]

The choice, moreover, allows a rigorous test of the proposed approach owing to the fact that the involved alumina polymorphs span a very large energy range, from about 4.50 eV to about 9.0 eV, of band gap values.

2. THE BASIS OF THE GENERALIZED SEMIEMPIRICAL APPROACH

In previous works,[27,32] we presented the details of our semiempirical approach from which eqs 1−3 were derived. According to this, we were able to derive the following relationships for the two parameters A and B of eq 1

$$A = 2\,E_I \quad (4a)$$

$$B = \frac{1}{y}[(D_{M-M} + yD_{O-O}) - R_{MO_y}] \quad (4b)$$

where, according to Phillips' suggestion,[49] the parameter E_I is assumed "to vary with the hybridization configuration, i.e., with different atomic coordinations in different crystal structures", D_{M-M} and D_{O-O} are the enthalpies of dissociation (bond strengths) of M_2 and O_2 in the gaseous phase, and R_{MO_y} is the repulsive term of the MO_y binary oxide. By neglecting the London components in the repulsive term, we can write

$$R_{MO_y} = (|U_{bond}| - |U_{lattice}|) \propto (d_{M-O})^{-2} \quad (5)$$

In the ionic limit, U_{bond} coincides with the Madelung energy, U_M, while in the covalent limit, a quantum mechanical calculation of the bonding energy is required. $U_{lattice}$ represents the experimental or calculated lattice energies of ionic solids.[50] According to the theory, a dependence from the inverse of the square of the anion−cation distance, d_{M-O}, has been assumed for R_{MO_y}.[51]

The problem of the variability of E_g values in the presence of different polymorphs was left unsolved in the initial work, but it has been recently afforded[32] in an attempt to extend the original approach to the case of nonregular ternary oxides containing both sp- and d-metal cations. We have shown that in several cases, the band gap value of different polymorphs of s,p- and d-metal oxides could be fitted by using eq 1 with fixed A and B values and by spanning χ in the entire range of χ_M values ($\chi_M = \chi_M^0 \pm 0.05$) accepted in deriving Pauling's scale of electronegativity.[34] As evidenced (see Table IV of our previous work),[32] a variation of ΔE_g in the order of 0.4−0.6 eV can be easily accounted for different polymorphs of d-metal

https://dx.doi.org/10.1021/acs.inorgchem.0c02691
Inorg. Chem. 2021, 60, 1419−1435

Table 1. Physical Data and A and B Parameters for Different Alumina Polymorphs[a]

polymorph/phase	volume per form. unit [Å^3]	density [g cm^{-3}][72]	$E_{g,exp}$ [eV]	$E_{g,DFT}$ [eV][52]	B	A	χ_{Al}
α-Al_2O_3	40.99[61] /42.52−42.60[52,55]	3.99	8.50[53]	8.60(d)	−2.71	2.80	1.50
κ-	43.28[61] /44.89[79]	3.98		7.40(d)	−2.415/−2.43	2.454/2.457	1.50
(β/θ)-	46.96−45.35[55,70,80,81] /45.04[61]	3.60−3.65	6.70(i)/7.05 (EELS)[82]	6.90(i)	−2.19/−2.26	2.27/2.24	1.50
γ(spinel)-	44.35[61] /45.25[59]	3.67	6.97(d)/6.86(i)[85] 3.35[57]	6.20(i)	−2.28	2.123/2.11	1.50
γ(paglia)-[52]	46.42[83] /46.98[84]		7.60[63] /7.00 (EELS)[56]	5.20	−2.23	2.265/2.25	
η-	46.47[83]	3.65		4.40	−2.25	1.66	1.50
am-ALD/spray pyrolysis		3.60[86,87]	6.70 (EELS)[80,81,88,89]	5.60/6.30[91]	−2.14	2.21	1.50
am-ALCVD/sputtering			5.62(i)[90]			1.94	
am-anodic thick film			6.30(i)[69]	2.50/3.00[77]		2.11	
anodic thin film		3.30/3.77[86,92,93]	4.60 (Tauc)[65]		−1.77/−2.40	1.60/1.75	1.50

[a]Direct (d) and indirect (i) band gaps.

oxides, showing a range of electronegativity values of $1.2 \leq \chi_M \leq 1.90$. For s,p-metal oxides spanning the same range of χ values, a wider range of ΔE_g values (0.7−1.0 eV) can be accommodated for different polymorphs going from more to less electronegative s,p cation.

In the case of alumina polymorphs, band gap values ranging from 5.54 eV to about 6.41 eV are obtained by using eq 1 with the A_{sp} and B_{sp} above reported and a $\chi_{Al} = 1.5 \pm 0.05$ value. Both of these values do not cover the range of band gap values reported in the literature for the different alumina polymorphs (see Table 1). To extend the limits of eq 1, it appears necessary to take into account, for different polymorphs, possible variations of A and B values around the experimental ones derived according to eq 1. According to Phillips's suggestion, E_I can be assumed to be dependent on the crystalline structure so that by keeping the variability of χ within the uncertainty range of Pauling's scale, it seems reasonable to hypothesize a variation in the A values (see eq 4a) with the nature of different polymorphs too. Moreover, according to eq 5, different values of the repulsive term R_{MO_y} and then of B values could be associated to different MO_y polymorphs as a consequence of their different crystalline structure. To check the validity of the previous assumptions, we will carry out the modeling of the optical band gap of ternary systems as a function of their composition with the aim of illustrating how to face with the problem of the band gap values of different polymorphs and in the presence of $E_{g,opt}$ data spanning a range of experimental values well above that estimated according to eqs 1−3 once the accepted range (±0.05 unit) of variability in χ_M is also accounted for.

With this aim, we identified several ternary systems of variable composition $xMO_y + (1 - x)AlO_{1.5}$, covering all the ranges of experimental and theoretically estimated optical gap values of alumina polymorphs,[52−65] as the most challenging test to our assumptions. However, for the sake of brevity, in this work, we will discuss the results pertaining to a few ternary oxides containing, apart from Al, both sp (Ga) and d-metals (Ta, Nb, and W).[43,66,67] Both crystalline ternary polymorphs and amorphous ternary oxides will be taken into account to test the ability of the proposed approach to model reliably the experimentally derived band gap values.

3. MODELING THE OPTICAL BAND GAP OF TERNARY OXIDE SYSTEMS

In a previous work,[32] we derived a generalized modeling equation of the optical band gap of ternary oxides by extending the results previously obtained for regular (sp,sp- or d,d-metals) mixed oxides to the nonregular (s,p-TM metals) mixed oxides. For nonregular ternary oxides, the band gap value, $E_{g,nr}$, of mixed oxide was derived from an extension of eq 1 and by using as a starting equation the following relationship

$$E_{g,nr} = x_1 E_{g,1}(\chi_{av}) + x_2 E_{g,2}(\chi_{av}) = E_{g,2}(\chi_{av}) + x_1(E_{g,1}(\chi_{av}) - E_{g,2}(\chi_{av})) \quad (6)$$

where

$$E_{g,1}(\chi_{av}) = A_1(\chi_O - \chi_{av})^2 + B_1 \quad (7a)$$

and

$$E_{g,2}(\chi_{av}) = A_2(\chi_O - \chi_{av})^2 + B_2 \quad (7b)$$

with

$$\chi_{av} = x_1\chi_1 + x_2\chi_2 \quad \text{and} \quad x_1 + x_2 = 1 \quad (7c)$$

with x_i and χ_i representing the cationic fraction (in at %) and Pauling's electronegativity parameter, respectively, of each metal M_i present in the mixed oxides. $E_{g,1}$ and $E_{g,2}$ represent the band gap values of pure binary oxides assumed to follow one of the two previous correlations (sp-sp or d-d-metal) according to eqs 1−3.

After substitution of eqs 7a−7c in eq 6 and rather simple algebraic manipulations, we got the equation for a generic ternary oxide system as

$$E_{g,nr}(\chi_{av}) = E_{g,2} + S_l x_1 + S_q x_1^2 + S_c x_1^3 \quad (8a)$$

where $E_{g,2}$ is the band gap of the pure oxide corresponding to $x_1 = 0$ and

$$S_l = 2A_2(\chi_O - \chi_2)(\chi_2 - \chi_1) + (B_1 - B_2) + (A_1 - A_2)(\chi_O - \chi_2)^2 \quad (8b)$$

$$S_q = 2(A_1 - A_2)(\chi_O - \chi_2)(\chi_2 - \chi_1) + A_2(\chi_1 - \chi_2)^2 \quad (8c)$$

$$S_c = (A_1 - A_2)(\chi_1 - \chi_2)^2 \quad (8d)$$

It is worth noting that whenever $A_1 = A_2$ and $B_1 = B_2$, i.e., if the two oxides M_1O_{y1} and M_2O_{y2} follow the same (d,d) or (sp,sp) correlation, the coefficient S_c becomes zero and we obtain the relationships used for fitting of the band gap values of regular ternary d,d and sp,sp-metal mixed oxides.[29,30,32] For

https://dx.doi.org/10.1021/acs.inorgchem.0c02691
Inorg. Chem. 2021, 60, 1419−1435

a regular ternary oxide ($S_c = 0$), we can define a bowing coefficient as

$$b = S_q = A(\chi_1 - \chi_2)^2 \quad (9)$$

Equations 8a–8d represent, however, more general relationships useful for modeling ternary systems where one or both pure oxides exist as different polymorphs spanning a large range of optical band gap values, which cannot be estimated with the initial correlation (see eq 1) by keeping constant the A and B parameters reported in eqs 2 and 3. Moreover, a more general expression is now obtained for the bowing coefficient, which could help fit a larger class of mixed semiconductor alloys, changing their crystallographic structure as a function of the composition.

3.1. Modeling the Optical Band Gap of Al_2O_3 and Ga_2O_3 Polymorphs and Their Pseudoregular Ternary Systems: α-$(Ga_{(1-x)}Al_x)_2O_3$ and β-$(Ga_{(1-x)}Al_x)_2O_3$.

To reduce the arbitrariness in the derivation of the A and B parameters for the different alumina polymorphs, we will assume as a reference for the different polymorphs the experimental $E_{g,opt}$ values estimated by optical techniques, whenever available, or the $E_{g,th}$ theoretical values recently reported by Peintinger et al.[52] This choice is supported by the fact that the investigated polymorphs are quite numerous and the E_g values are, in many cases, in good agreement with those experimentally obtained by different research groups using also different techniques.

As mentioned above, in the presence of different polymorphs, the value of the two parameters A and B, necessary to estimate the E_g value according to eq 1, can differ from those derived from the best fitting procedure.[27] This can be attributed to the fact that in different crystalline structures, both the coefficient E_I and the repulsive energy term R_{MO_y} can assume different values for different polymorphs.

As for Al_2O_3, a band gap value of 6.3 ± 0.1 eV was used for alumina, as derived from photocurrent spectroscopy measurements of a thick amorphous anodic alumina film.[27,68,69] It is encouraging that an indirect band gap value of 6.2 eV has been derived very recently by Peintinger et al. for the γ-Al_2O_3 polymorph[52] as well as by Liu et al. for amorphous alumina.[70] It is known that anodic alumina crystallizes as γ-Al_2O_3 at not too high temperature[71] (450 °C) or under an electron beam of a transmission electron microscope during extended observation.[72] However, the band gap values of $\alpha,\kappa,\theta,\eta$-$Al_2O_3$ are outside the range of values accessible with the proposed correlation so that a search for the right values of $A_{(\alpha,\kappa,\theta,\text{-Al2O3})}$ and $B_{(\alpha,\kappa,\theta,\text{-Al2O3})}$ is necessary if we want to fit the ternary systems α-$(Ga_{(1-x)}Al_x)_2O_3$ and β-$(Ga_{(1-x)}Al_x)_2O_3$) for which $E_{g,opt}$ values between 7.80 eV (α-phase) and 6.50 eV (β-phase), respectively, have been reported in the literature[73,74] in the presence of Al at % content into the oxide well below 100% ($x \approx 0.70–0.80$) (see also Figures 1 and 2).

To fit the series of experimental and/or theoretical data for both ternary polymorph systems, we need to obtain further information on the possible changes in A and B values for the different gallia and alumina polymorphs. As mentioned above, by looking into the expression of B reported in eq 4b, it shows that the only term affecting the B parameter can be traced out to the repulsive energy term R_{MO_y} usually assumed to depend from the inverse of the square of the anion–cation average distance.[51]

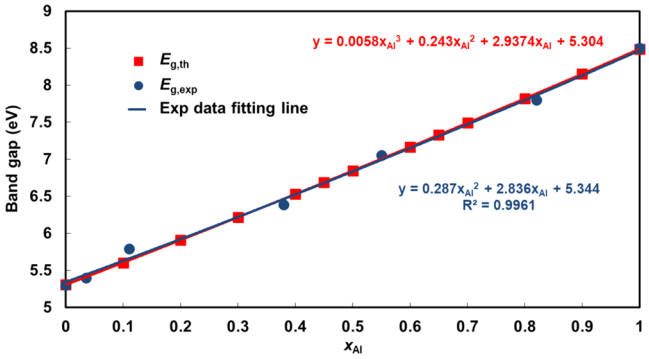

Figure 1. Experimental direct optical band gap values[73] of α-$(Ga_{(1-x)}Al_x)_2O_3$ ternary system vs Al content ($0.03 \le x_{Al} \le 0.81$) (blue circles). Theoretical data points derived according to eqs 8a–8d and by assuming the following (see text): $\chi_{Al} = 1.50$; $B_{\alpha\text{-Al2O3}} = -2.71$ eV; $A_{\alpha\text{-Al2O3}} = 2.80$; $\chi_{Ga} = 1.60$; $B_{\alpha\text{-Ga2O3}} = -2.71$ eV; $A_{\alpha\text{-Ga2O3}} = 2.22$ (red squares).

Regarding the different alumina and gallia polymorphs, α-Al_2O_3 and α-Ga_2O_3 display the lowest volume per formula unit[52,61,70,75] so that it seems reasonable attributing the highest (absolute value) B_{sp} value of −2.71 to this polymorph. Moreover, by assuming as a proxy of anion–cation average distance the cubic root of the unit formula volume, we corrected the B term of each polymorph, B^i, by the ratio $r_v = (V^\alpha/V^i)^{2/3}$. According to this, and by using eqs 4b and 5, each B^i value, for a different polymorph, was obtained through the relationship

$$B^i = B^\alpha + (R_{(\alpha-MO_y)}/y) \times [1 - (V^\alpha/V^i)^{2/3}] \quad (10a)$$

where B^i, V^i, B^α, and V^α represent respectively the B parameter and the unit formula volume of the ith-polymorph and of the α-phase. As for the repulsive energy term $(R_{(\alpha\text{-}MO_y)}/y)$, the values of 8 and 7.27 eV were estimated from the literature data[76] for α-alumina and β-gallia, respectively.

According to this, whenever reliable unit volume data were at our disposal and in the presence of appreciable variation in the volume ratio ($r_v > 2\%$) of the different polymorphs, we carried out a correction to the B^i parameter value reported in eqs 2 and 3 for s,p-metals and d-metal oxides, respectively. Moreover, the A term of each polymorph was adjusted as a function of the repulsive term, through eq 1, by using the estimated B values according to eq 10a and by keeping constant, as a first choice, the EN value χ_M^0 of the metal for all polymorphs. Values of A obtained according to this procedure seem to be more physically acceptable than the choice of fitting the experimental data reported in Figures 1 and 2 (see below) by assuming a constant electronegativity parameter for both β-phase and α-phase as a constraint and leaving both B and A as free variables.

As for the gallia polymorphs ($\alpha,\beta,\gamma,\delta,\kappa/\varepsilon$-$Ga_2O_3$), for which reliable optical band gap values (5.20–5.30 eV for α and 4.40–4.90 eV for the $\beta,\gamma,\delta,\kappa$-phase) (see Table 2) have been reported in the literature,[70] we like to stress that almost all band gap values (between 4.70 and 5.50 eV) can be derived through eq 1 by using the A and B parameters reported for s,p-oxides (eq 3) and an EN parameter $\chi_{Ga} = 1.60 \pm 0.05$ as reported in Pauling's scale.[34] A range of $E_{g,opt}$ values (5.12 ± 0.42 eV), in good agreement with the range of optical band gap values reported in the literature for all different polymorphs,

https://dx.doi.org/10.1021/acs.inorgchem.0c02691
Inorg. Chem. 2021, 60, 1419–1435

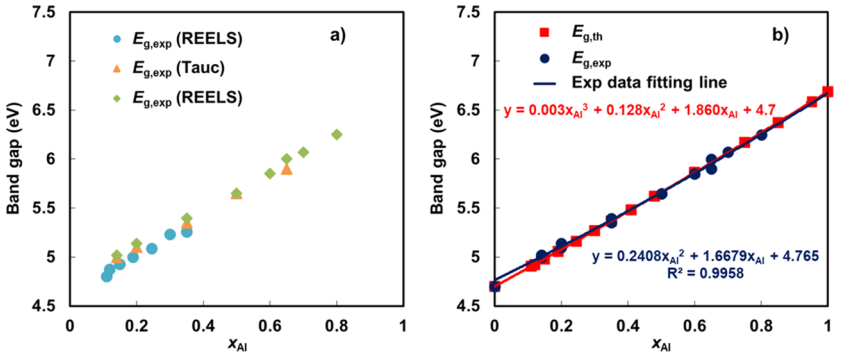

Figure 2. (a) Band gap values of β-$(Ga_{(1-x)}Al_x)_2O_3$ ternary system vs Al content ($0.11 \leq x_{Al} \leq 0.81$) for experimental data points (polycrystalline powders[74] and PLD films[116]) derived from the REELS (circles and diamonds) technique and Tauc plot from optical absorption measurements on the PLD film[101] (triangles, see text). (b) Experimental band gap values from REELS data of β-$(Ga_{(1-x)}Al_x)_2O_3$ ternary system vs Al content ($0.11 \leq x_{Al} \leq 0.81$) (blue circles). Theoretical data points derived according to eqs 8a−8d and by assuming the following (see text): $\chi_{Al} = 1.50$; $B_{\theta\text{-}Al2O3} = -2.225$ eV; $A_{\theta\text{-}Al2O3} = 2.23$; $\chi_{Ga} = 1.60$; $B_{\beta\text{-}Ga2O3} = -2.31$ eV; $A_{\beta\text{-}Ga2O3} = 1.96$ (red squares).

Table 2. Physical Data and *A* and *B* Parameters for Different Gallia Polymorphs[a]

polymorph/phase	density [g cm^{-3}][97]	volume per form. unit [Å^3]	$E_{g,exp}$ [eV]	$E_{g,DFT}$ [eV]	B	A	χ_{Ga}
α-Ga_2O_3 trigonal	6.47	48.48[75]	5.30[73]	5.40(i)/5.60(d)[75]	−2.71	2.22	1.60
				5.25(i)[98] /5.34(d)[99]		2.17	1.576
β-Ga_2O_3 monoclinic	5.9	52.84[75] /52.21[100]	4.75(i)/4.85(d)[101]	5.00(i)(d)[75]	−2.28	1.95(i)/ 1.98(d)	1.60
				4.69(d)[98]			
				4.87(i)(d)[99]	−2.34	1.97(i)/ 2.00(d)	
γ-Ga_2O_3 cubic-defective-spinel	6.05	51.84	4.80(i)/4.96(d)[85]				1.60
					−2.39	2.00(i)/ 2.04(d)	
κ,ε-Ga_2O_3 orthorhombic	5.88	51.09[75] /52.94[102]	4.95 ± 0.05(d)[97,102−104]	4.84(d)[105]	−2.45	2.05	1.60
					−2.33	2.02	

[a]Direct (d) and indirect (i) band gaps.

can be derived by keeping the χ_{Ga} value within the uncertainty limit of Pauling's scale of electronegativity.

In fitting the experimental optical band gap data of crystalline oxide, we will use for different polymorphs the *B* values reported in Tables 1 and 2 derived according to eq 10a. In the case of amorphous phases or in the absence of information on the value of unit formula volume, V^i, a similar approach as devised in eq 10b, but based on the data density ρ of the anodic film or other noncrystalline phases,[71,77,78] was adopted to get the *B* parameter as follows

$$B^i = B^\alpha + R_{(\alpha-MO_y)} \times [1 - (\rho^\alpha/\rho^i)^{-2/3}] \quad (10b)$$

where ρ^α and ρ^i are the densities of α and *i*-phase, respectively.

In Table 1, the E_g value for five polymorphs of Al_2O_3, theoretically derived from DFT methods[52] and covering all the ranges of expected band gap values, are reported. In the same table, we reported the *A* and *B* values, the latter of which was estimated through eqs 10a and 10b and the former through eq 1 by using the calculated *B* and the chosen theoretical or experimental E_g value.

We stressed above that γ-Al_2O_3 (E_g = 6.20 eV) is the one that follows eq 1 by using the average *A* and *B* values of the semiempirical correlation valid for s,p-oxides. After correction of the *B* value according to eqs 10a and 10b ($B = -2.30$ eV), a value of E_g = 6.20 eV is obtained for such a polymorph with χ_{Al} = 1.52 and $A = 2.17$.

It is evident that the decrease in *B* value is now compensated, at a fixed *A* parameter, by the small variation in the electronegativity parameter well within the confidence limits of Pauling's scale of electronegativity (≤0.05). At fixed $\chi_{Al} = 1.50$, a very small variation in the value of *A* (2.15 ± 0.025) is sufficient to get a very nice agreement between estimated (6.30 ± 0.1 eV)[69] and band gap values of γ-Al_2O_3 reported by Peintinger et al.[52]

As for θ-Al_2O_3, a good agreement is found between the DFT-estimated E_g value (6.57[70] −6.90 eV) and that one obtained ($E_{g,opt}$ = 6.70 eV) according to eq 1 by using the new value of *B* (−2.22 eV) and a slightly higher *A* value (2.23) by keeping χ_{Al} = 1.50 constant. The last $E_{g,opt}$ value is the experimental optical band gap of θ-Al_2O_3 obtained by Tauc plot analysis in the hypothesis of indirect optical transitions (see below). We like to stress that if we assume for θ-Al_2O_3 the DFT-based value[52] of Table 1 ($E_{g,th}$ = 6.90 eV), a value of 2.17 for the parameter *A* is still compatible with the E_g value of 6.90 eV provided that a value of χ_{Al} = 1.45, still within the accepted EN variability, is assumed for Al in this polymorph.

From this short analysis of the data, it shows that eq 1 is able to fit the band gap values of the two most common alumina polymorphs (γ,θ-Al_2O_3) by using the average *A* value for s,p-metal oxides together with the χ^0_{Al} value reported in the classical Pauling's book and in agreement with the confidence limits of Pauling's scale of electronegativity.

As for the other two polymorphs (α,κ-Al_2O_3) reported in Table 1, showing the highest band gap values, we derived

https://dx.doi.org/10.1021/acs.inorgchem.0c02691
Inorg. Chem. 2021, 60, 1419−1435

values of A parameter well above the average value of s,p-metal oxides. For the α-Al_2O_3 polymorph, a value of A = 2.80 is required to fit the experimental band gap value[53] of 8.50 eV by assuming χ_{Al} = 1.5. For κ-Al_2O_3, a slightly lower A value (2.46) is required to fit the band gap value of 7.40 eV by using the new B value of −2.45 eV. The observed increase in the values of A_{sp}, with a corresponding increase in Phillips' parameter E_I (see eqs 1−3), could be attributed to the presence of stronger Al−O average bonds along the series of polymorphs: $\alpha > \kappa > \theta \approx \gamma$. As recently reported by Filatova and Konashuk,[63] the widening of the band gap of alumina polymorphs, from γ-Al_2O_3 to α-Al_2O_3, is mainly due to the shift of the bottom of the conduction band (CB) (≥1.37 eV) in the presence of a very negligible shift in the maximum of the valence band (VB) (around 0.17 eV between α-Al_2O_3 and γ-Al_2O_3). Such a large shift of CB has been shown to be governed by the charge transfer from Al to oxygen, which is strongly dependent on the local Al coordination symmetries. Octahedral coordination of Al ions favors a larger shift of CB bottom with respect to the tetrahedral coordination and such a suggestion agrees with the experimental findings showing that in a corundum structure of α-alumina, Al ions occupy only octahedral sites, while both octahedral and tetrahedral sites are occupied in γ-alumina. Analogous considerations could be valid for the corresponding gallia polymorphs where, however, a smaller difference in the E_g values is reported between α-Ga_2O_3 and γ-Ga_2O_3 (see Table 2). A possible rationale for this finding could be related to the smaller difference in electronegativity between oxygen and Ga ($\Delta\chi_{(Ga)}$ = 1.9 vs $\Delta\chi_{(Al)}$ = 2.0), which could account for the smaller range of experimental E_g values reported for the different gallia polymorphs (see Table 2).

Among the polymorphs considered in Table 1, the most intriguing aspects are those related to the η-phase, for which a DFT-derived E_g value of 4.40 eV has been reported.[52] As discussed in the literature, η-alumina, with respect to the other polymorphs, is a less ordered and more defective crystalline phase for which no experimental E_g value has been reported up to know, at our best knowledge. The lower E_g value reported for this polymorph, with respect to all other polymorphs, should agree with the suggestions made by different authors[59,60,77,78,94,95] that both the degree of disorder and the density of different polymorphs affect their band gap values through the ion coordination number and the bond length of different structural units. Reasonably, both the density and the disorder degree affect the band gap by weakening the Al−O average bond energy. To fit a very low band gap value, in the presence of an appreciably lower (−2.2 ± 0.05 eV) B value, a larger decrease in the A value (1.67−1.78), with respect to the average one, is required by using electronegativity values in the range of χ_{Al} = 1.50−1.55.

For α-Ga_2O_3, if we assume the most common reported value[96] of 5.30 eV for $E_{g,opt}$, a value of χ_{Ga} = 1.578, very close to Pauling's value of 1.60, is obtained from eq 1 by using the average A and B values of s,p-oxides. On the other hand, by assuming the value of χ_{Ga} = 1.60, a value of A = 2.22 (+2.3%) is obtained by keeping E_g and B constant. As for the β-Ga_2O_3 polymorph, owing to the large ranges of band gap values reported in the literature, the more detailed discussion underlying the choice of E_g value will be presented in the following section.

3.2. Fitting of the Pseudoregular Ternary sp-sp Oxide Band Gap.

3.2.1. α-$(Ga_{(1-x)}Al_x)_2O_3$ Ternary System. Although eqs 8a−8d have been derived for nonregular (sp,d-metal mixed oxide) ternary oxides, they can be used also for "pseudoregular" ternary systems where one or both binary oxides, although belonging to the same correlation, are present as a polymorph whose band gap value could be different with respect to that calculated through eq 1.

In Figure 1, we report the experimental data (blue full circles) of direct optical band gap values,[73] $E_{g,dir}$, derived for crystalline films of corundum-like polymorphs (α-$(Ga_{(1-x)}Al_x)_2O_3$) covering almost the entire compositional range: $x_{Al} \leq 0.81$.

The experimental $E_{g,opt}$ values of pure oxides, $E_{g2} = E_{g,\alpha\text{-}Ga2O3}$ and $E_{g1} = E_{g,\alpha\text{-}Al2O3}$, have been fixed as 5.30 eV[96] and 8.50 eV,[53] respectively. This last value is in good agreement with recent experimental values, obtained by the REELS technique (8.40[64]−8.70 eV[58]) or optical absorption[106] (E_g = 8.60 eV), as well as with the theoretical ones (E_g = 8.56−8.80 eV)[52,98,99,107] derived from DFT-based techniques.

As for α-Ga_2O_3 (x = 0, in Figure 1), optical band gap values between 5.17 and 5.60 eV have been reported in the literature.[108−110] The direct optical band gap value of 5.30 eV, obtained by means of a Tauc plot,[96] has been chosen in Figure 1. The best fitting quadratic line of the experimental data is

$$E_{g,dir} = 0.287x_{Al}^{\ 2} + 2.836x_{Al} + 5.344\ [eV] \quad (11a)$$

To fit the experimental data set points by using eqs 8a−8d, we need to derive the A and B values of Tables 1 and 2 and Pauling's EN values of Al (1.50) and Ga (1.60). By assuming B = −2.71 eV for both α-polymorphs, A values of 2.80 and 2.22 were derived for α-Al_2O_3 and α-Ga_2O_3, respectively, by using eq 1 with the assumed E_g values. The theoretical points (red full squares in Figure 1) have been estimated through the following equation

$$E_{g,th} = 0.0058x_{Al}^{\ 3} + 0.243x_{Al}^{\ 2} + 2.9374x_{Al} + 5.304[eV] \quad (11b)$$

by using the parameter discussed above and reported in captions. Very good accordance is reported with the experimental data, demonstrating the reliability of our approach.

We like to stress that the bowing coefficient of the fitting curve related to experimental data (b = 0.287 eV, see eq 11a) is much smaller than the theoretical values recently reported by Weng et al.[98] (b = 1.60) and Peelaers et al.[99] (b = 1.87), derived by using for α-$(Ga_{(1-x)}Al_x)_2O_3$ the $E_g(x_{Al})$ values calculated by DFT techniques, but it is in very good agreement with the S_q value (0.243) calculated according to eq 8c. Although further investigations are necessary on these aspects, before reaching final conclusions, the very nice agreement between experimental and theoretically estimated E_g and bowing coefficient values is a strong support in favor of the suggested approach. It also shows that eq 11b can be reliably used to estimate the E_g values of α-$(Ga_{(1-x)}Al_x)_2O_3$ or indirectly estimate the composition of the mixed oxide by knowing the band gap value.

3.2.2. β-$((Ga_{(1-x)}Al_x)_2O_3)$ Ternary System: E_g vs x_{Al} for Indirect Optical Transitions. Much more complications arise for the second pseudoregular ternary system β-$(Ga_{(1-x)}Al_x)_2O_3$ since largely variable E_g values have been reported in the literature for the band gap of β-Ga_2O_3 (4.4−5.0 eV)[35,36,111−113] as well as for ternary β-$(Ga_{(1-x)}Al_x)_2O_3$ mixed oxides as a function of different methods of preparation

https://dx.doi.org/10.1021/acs.inorgchem.0c02691
Inorg. Chem. 2021, 60, 1419−1435

and techniques of evaluation of the band gap.[37−39,74,101,114−122] Usually, lower optical band gap values are measured in the Tauc plot by assuming indirect optical transitions, while larger values are measured in the hypothesis of direct optical transitions.[101] Still, different values have been reported in the case of E_g values estimated by using ellipsometry or the REELS technique.[74,101,114−121] In some cases, nearly identical E_g values have been reported by using REELS or the Tauc method of determination of band gap, but large scattering of data has been reported from the same laboratory.[119,120]

No experimental data, unfortunately, have been reported in the literature for the band gap of single crystal θ-Al_2O_3, at our best knowledge, while different theoretical band gap values have been calculated by using DFT-based techniques. According to more recent works, direct band gap values of 6.57[95] and 7.51 eV[99] and indirect ones of 6.90,[52] 7.03,[98] and 7.24 eV[99] have been suggested for θ-Al_2O_3.

As for the fitting of β-$(Ga_{(1-x)}Al_x)_2O_3$ experimental data, in Figure 2a, we reported the experimental E_g data of β-$(Ga_{(1-x)}Al_x)_2O_3$ films of variable composition and deposited by different techniques: atomic layer deposition (ALD), pulsed laser deposition (PLD), and RF-magnetron sputtered deposition.[101,114−121]

The band gap of these films was derived from REELS (orange triangles) or optical techniques through the Tauc plot (azure circles) in the hypothesis of indirect optical transitions.[101] The band gap values, obtained by the REELS technique, of polycrystalline powders grown by solution combustion synthesis[74] are also reported in Figure 2a (green diamonds). The difference (≤0.1 eV) in the E_g values observed in the low composition range ($x_{Al} \leq 0.35$) can be reasonably attributed to the different techniques employed to extract the band gap value.

On the other hand, the data represented by triangle and diamond symbols in Figure 2a pertain to PLD films and crystalline powders, respectively, for which the band gap values have been obtained by the same REELS technique.[74,116] The $E_{g,REELS}$ vs x_{Al} data set (dark blue symbols in Figure 2b) pertaining to both polycrystalline powders and PLD films will be assumed as the "reference data set" owing to the larger interval of composition covered ($0.11 \leq x \leq 0.81$) as well as to the good reproducibility of the REELS data derived from different laboratories and for samples grown by different techniques.

For the considered experimental data, the equation of the best fitting line is

$$E_{g(REELS)} = 1.8695x_{Al} + 4.7361[eV] \quad (12a)$$

with $E_{g,1}$ = 6.60 eV (x = 1) in the hypothesis of a linear fit. By assuming a second-order fitting equation, the best fitting line is

$$E_{g(REELS)} = 0.3623x_{Al}^2 + 1.55x_{Al} + 4.789[eV] \quad (12b)$$

with $E_{g,1}$ = 6.70 eV. We have to mention that the large differences in the linear terms observed in the previous fitting lines must be attributed to the fact that no constraints were imposed to the band gap values, E_{g1} and E_{g2}, of pure oxides. The linear fitting equation is almost coincident with that reported by Krueger et al.[74] and Fares et al.,[116] while the parabolic fitting gives, once again, a bowing coefficient much smaller than that reported by Wang et al.[98] (b = 1.0 eV/x^2) and Van de Walle et al.[99] (b = 0.93). As for θ-Al_2O_3, the dispersion in the DFT-calculated $E_{g,ind}$ values is smaller than for $E_{g,dir}$, but the DFT-estimated values ($E_{g,ind}$ = 6.90−7.25 eV)[52,98,99] are appreciably higher than the value of θ-Al_2O_3 band gap (6.60−6.70 eV) obtained by extrapolation to x = 1 from eqs 12a and 12b, pertaining to the "reference data set".

As mentioned above, the $E_{g,REELS}$ values in the low x region ($x_{Al} \leq 0.35$) are quite close to the indirect optical band gap values derived from Tauc plots so that it seems reasonable to use as an end point in the fitting process (E_{g2} in eq 8a) an E_g value of β-Ga_2O_3 obtained by the same (REELS and Tauc plot) techniques. If we fix the E_{g2} value for β-Ga_2O_3 by assuming a value of 4.75 eV, i.e., an average value of experimental E_g data reported in the literature for $E_{g,ind}$ of β-Ga_2O_3, the fitting lines equations now become

$$E_{g,\beta-(Ga(1-x)Alx)2O3} = 1.8624x_{Al} + 4.74\ [eV];\ E_{g1} = 6.60\ eV \quad (12c)$$

$$E_{g,\beta-(Ga(1-x)Alx)2O3} = 0.2408x_{Al}^2 + 1.667x_{Al} + 4.765\ [eV];\ E_{g1} = 6.67\ eV \quad (12d)$$

A change in the bowing parameter from b = 0.3623 eV/x^2 to b = 0.241 eV/x^2 is now recorded going from eq 12b to eq 12d, with a consequent better agreement in the linear terms of eq 12c (S_l = 1.8624 eV/x) and eq 12d (S_l = 1.668 eV/x). A value of $E_{g,ind}$ = 6.67 eV is obtained for θ-Al_2O_3 by extrapolating to x = 1, in good agreement with the frequently reported REELS band gap values of 6.8 ± 0.2 eV measured for ALD Al_2O_3 films.[82,115,123] This value is in good agreement also with that estimated by Peintinger et al. and is reported in Table 1.

The fitting of experimental $E_{g,REELS}$ data was carried out according to eqs 8a−8d (see red squares in Figure 2b) by using the standard Pauling's electronegativity values of χ_{Ga} = 1.60 and χ_{Al} = 1.50 and the B values of −2.32 and −2.25 eV (see Tables 1 and 2) for β-gallia and θ-alumina, respectively. The value of A parameter for β-gallia ($A_{\beta\text{-}Ga2O3}$ = 1.96) was derived according to eq 1 by using the band gap value of 4.75 eV for β-gallia. The theoretical points calculated according to eqs 8a−8d by using $A_{\theta\text{-}Al2O3}$ = 2.23 nicely fits the experimental data point, providing the following theoretical equation

$$E_{g,th} = 0.0029x_{Al}^3 + 0.1278x_{Al}^2 + 1.8598x_{Al} + 4.7\ [eV] \quad (12e)$$

From eq 12e, a value of E_{g1} = 6.69 eV for pure θ-Al_2O_3 was obtained by extrapolating to x = 1. This value is in very good agreement with the REELS band gap value (6.80 ± 0.2 eV) estimated for pure Al_2O_3 ALD films[123] and with the value of about 7.05 eV estimated for a very thin film of θ-Al_2O_3 obtained by thermal treatment at 1200 K of an initial amorphous film.[82] As for the bowing parameter value, a good agreement is observed between the experimental one (0.241 eV/x^2) and theoretical one (0.1278 eV/x^2). As for the A values of the two polymorphs, a negligible increase (+3%) for θ-Al_2O_3 and a more appreciable decrease (−10%) for β-Ga_2O_3 are observed with respect to the average A value (2.17) of s,p-metal oxides.

To stress the validity of the chosen fitting strategy, consisting in the use of a reduced number of experimental data set but covering the largest compositional range, where the metastable

https://dx.doi.org/10.1021/acs.inorgchem.0c02691
Inorg. Chem. 2021, 60, 1419−1435

monoclinic structure of β-$(Ga_{(1-x)}Al_x)_2O_3$ exists, we reported in the Supporting Information (Figure S1) the fitting equation derived by using all experimental data sets of $E_{g,exp}$ vs x_{Al} values including all samples and band gap values regardless of the method of preparation and technique of E_g measurement. In the case of E_g optical values, the $E_{g,dir}$ data, derived from the Tauc method, were used, although no relevant change occurred in the fitting equation if $E_{g,ind}$ data were used. A value of the bowing parameter very near 0.46 was obtained in both cases. It is worth noting that the E_g values, estimated by using the fitting equation of theoretical data, differ by less than 0.1 eV from those estimated by using the fitting equation derived in Figure S1 in all ranges of composition exploited ($0 \leq x_{Al} \leq 0.81$). In the Supporting Information, we report also the fitting of the experimental data set[101] of direct optical band gap values, $E_{g,dir}$ vs x_{Al}, by keeping constant the B values of β-polymorphs and the EN values for Ga and Al, showing that a small increase (in the order of 1−3% for β-$(Ga_{(1-x)}Al_x)_2O_3$) in the A values employed in Figure 2 is able to fit the experimental data.

3.3. Fitting of the Nonregular Amorphous Ternary Oxide Band Gap. In previous sections, we tested the ability of our semiempirical approach in modeling the band gap of crystalline ternary oxides by considering also the influence of different polymorphs in determining the band gap of pseudoregular ternary oxides. In this section, we will take into account how to extend our approach to the case of amorphous nonregular ternary oxides. With this aim, we will take advantage of our previous studies on the photoelectrochemical characterization of anodic oxide films grown on pure transition metals (TMs) and mixed Al-TM (TM = Nb, Ta, W, Ti, etc.) alloys playing an important role in passivity studies[43,66,67,124,125] as well as in microelectronics[4,126] and near-infrared interferometry equipment.[44]

In previous works, in the absence of a general semiempirical approach to the modeling of nonregular amorphous ternary systems, we proposed on a purely heuristic basis the fitting of the $E_{g,opt}$ vs x_{Al} data points of amorphous oxides anodically grown on magnetron-sputtered Al-TM alloys based on the use of eq 1 modified as

$$E_g = A(\chi_O - \chi_{M,av})^2 + B \tag{13a}$$

where $\chi_{M,av} = x_{Al}\chi_{Al} + x_{TM}\chi_{TM}$ and from which the value of A to be used in the bowing equation of mixed ternary oxide

$$E_g(x_{Al}) = E_{g,TMO_x} + 2A(\chi_{TM} - \chi_{Al})(\chi_O - \chi_{TM})x_{Al} + A(\chi_{Al} - \chi_{TM})^2 x_{Al}^2 \tag{13b}$$

was derived. Equation 13b follows from eqs 8a−8d whenever $A_1 = A_2 = A$ and $B_1 = B_2 = B$. As previously reported,[67] a good agreement was observed, for the am-$(Al_xNb_{(1-x)})_2O_{(5-2x)}$ ternary system, between the experimental $E_{g,opt}$ data and those estimated according to eq 13b by using $\chi_{Al} = 1.50$ and $\chi_{Nb} = 1.615$ as electronegativity values and $A = 2.145$. Analogously, for Al-Ta alloys, eq 13b was able to fit also the data of $E_{g,opt}$ vs the Al content once the values of $\chi_{Al} = 1.478$ and $\chi_{Ta} = 1.505$ were substituted in eq 13b, together with the value of $E_{g,Ta2O5}$ measured for passive films grown on pure magnetron-sputtered Ta. On the other hand, in the case of passive films grown on Al-W,[66] a value of $A = 1.35$ with $\chi_{Al} = 1.50$ and $\chi_W = 1.70$ was able to fit the experimental $E_{g,opt}$ vs x_{Al} data points. In spite of the good accordance between experimental and theoretically derived E_g values,[43,66,67] a close inspection of eq 13b evidences its limits with respect to the general approach on which eqs 8a−8d are based. In fact, eq 13b provides a constant identical band gap value for mixed sp,d-metal oxides having the equal EN parameter ($\chi_i = \chi_j$) in all ranges of composition including the pure oxides, at $x = 0$ and $x = 1$, at variance with the results of eqs 2 and 3. This inconvenience does not occur with eqs 8a−8d, in agreement with the general approach outlined above, and more importantly, we do not need to derive the new values of A to be used in eq 13b to estimate the $E_{g,opt}$ values of nonregular ternary mixed oxides.

With respect to the crystalline systems investigated in Section 3.2, in the case of Al-TM passive films, grown by anodizing on their respective bulk metals or magnetron-sputtered alloys, amorphous pure or mixed oxides were formed, provided that the anodizing process is stopped before the onset of electrical breakdown phenomena when a crystallization process can occur. It has been shown for different amorphous passive films on valve metals (Al, Ta, Nb, W, Ti, etc.) and their alloys[43,66,67] that during the anodization process, both anodizing current and final voltage, despite the fact the final anodizing voltage is kept below the onset of the electrical breakdown process, affect sensibly the measured optical band gap values of the amorphous anodic film.[127,128] Usually, amorphous thicker films, grown at a constant growth rate, or films grown at lower growth rates display lower optical band gap values with respect to thinner films or films grown at higher anodizing rates.[43,66,67]

In previous works,[31,32,43,66,67,128,129] we suggested as a possible rationale for these findings a different degree of amorphousness as a function of the different anodizing parameters. Our suggestion was in agreement with the model of electronic density of state (DOS) in amorphous semiconductors described in the classical Mott−Davis book[130] showing how a different degree of lattice disorder affects the DOS in the vicinity of the conduction and valence band edges.[128] This suggestion is supported by older and very recent structural studies showing the striking similarity existing in a short range order between amorphous and crystalline valve-metal oxides.[44−47,72,131−135] This is a rather special situation occurring in stoichiometric amorphous materials where the only crystallographic defect is the absence of a medium-long-range crystalline order, while a short-range order still exists. When this occurs, the mobility gap, E_{mg}, is given by the distance in energy between the conduction band mobility edge (E_{CM}) and valence band mobility edge (E_{VM}) in the sense of Mott−Davis.[130] E_{mg} is usually derived from the photocurrent spectra and Tauc plot analysis in the hypothesis of indirect (nondirect in the case of amorphous materials) optical transitions. We have shown that for amorphous anodic films grown on valve metals[31,43,128,136,137] (Ta, Nb, W, Ti, etc.), in not incorporating an electrolyte solution, the difference between the mobility gap and the optical band gap of the crystalline counterpart, $\Delta E_{am} = (E_{mg} - E_{g,cryst})$, can reach a value in the order of 0.3−0.4 eV. According to Mott−Davis, such a difference is a measure of the influence of lattice disorder on the measured optical band gap values of amorphous materials and, when it occurs, an exponential tail (Urbach tail) in the measured photocurrent, for photon energies lower than the mobility gap value ($h\nu < E_{mg}$), could be a signature of the existence of an exponential DOS

https://dx.doi.org/10.1021/acs.inorgchem.0c02691
Inorg. Chem. 2021, 60, 1419−1435

distribution of localized states at energies below the mobility edge.

In the Mott−Davis model of an amorphous semiconductor (SC), the ΔE_{am} term is essentially positive or zero, but we are aware that this term can turn to a negative value if, apart from the absence of long-range crystalline order, intense optical transitions originated by a distribution of vacant/filled electronic states (DOS distribution) within the mobility gap are occurring. In this case, the presence of other possible crystallographic defects as well as of impurities and/or nonstoichiometry has been suggested in the literature.[22−25,69,124,138−140]

It is important to note that with respect to the previous approach,[31,32] the relationship usually employed for amorphous oxide

$$E_{mg} - \Delta E_{am} = A(\chi_O - \chi_M)^2 + B \quad (14a)$$

will be modified, in the following, by introducing the term ΔE_{am} into the B value so that for an amorphous TM anodic film, eq 1 used in the fitting procedure becomes

$$E_{mg} = 1.35(\chi_O - \chi_M)^2 + B_{am} \quad (14b)$$

with $B_{am} = (-1.5 + \Delta E_{am})$. The value of ΔE_{am} will be derived, where possible, as the difference of optical band gap values between amorphous oxides and their crystalline polymorph counterparts. To account for the noticeable dependence of E_{mg} values, in amorphous SCs, from their method of preparation, different values of ΔE_{am} derived as mentioned above will be used in the fitting process for a fixed metal or alloy.

As for the choice of the alumina polymorph to be used as a partner, in fitting the experimental optical band gap values of the ternary investigated amorphous systems (am-$(Al_xNb_{(1-x)})_2O_{(5-2x)}$, am-$(Al_xTa_{(1-x)})_2O_{(5-2x)}$, and am-$(Al_{2x}W_{(1-x)})O_3$), the choice of η-alumina appears to be quite natural by taking into account that the investigated ternary anodic oxides are amorphous and that:

a η-Al_2O_3 is the metastable alumina polymorph with a crystallographic structure nearest to a disordered amorphous aluminum oxide for which a reliable optical band gap value has been estimated.[52]

b The preliminary best fitting procedures of the experimental $E_{g,opt}$ values vs x_{Al} ($0 \le x_{Al} \le 0.8$) of anodic films on these ternary systems provided band gap values for the pure anodic alumina film (estimated by extrapolating to $x = 1$) ranging between 4.33 eV, from the am-$Nb_{(1-x)}Al_x)_2O_{(5-2x)}$ system, and 4.47 eV, from the am-$Ta_{(1-x)}Al_x)_2O_{(5-2x)}$ system (see below Figures 3 and 4). It is noteworthy that both of these values differ only by ±0.07 eV from the 4.40 eV value estimated by Peintinger et al. for η-Al_2O_3. A slightly lower $E_{g,opt}$ value (4.24 eV) was derived for am-$(Al_{2x}W_{(1-x)})O_3$ covering a slightly lower compositional range ($x_{Al} \le 0.70$ into the film).

As far as we know, an experimental E_g value for η-Al_2O_3 has not yet been reported in the literature, but as reported in the literature, η-Al_2O_3 is a defective spinel structure[52,83,141] showing the lowest crystallinity and estimated $E_{g,opt}$ value between all the metastable alumina phases. According to this, η-alumina, with its largest unit formula volume, will be assumed as the reference structure for the calculation of the B parameter in the case of amorphous alumina for which largely variable densities (ρ = 2.35−3.60 g cm^{-3}) have been reported

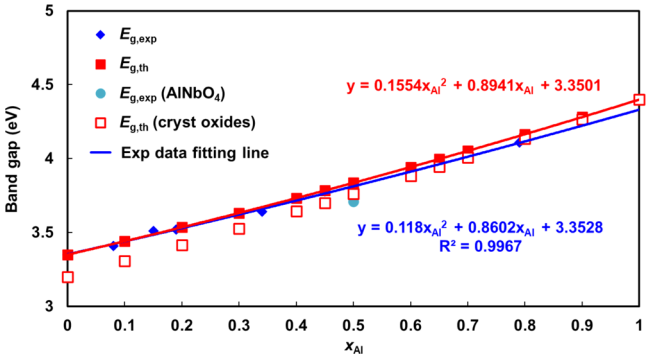

Figure 3. Nondirect optical band gap values vs Al content ($0 \le x_{Al} \le 0.8$) (azure diamonds) for amorphous anodic films grown on Al-Nb magnetron-sputtered alloys of various compositions derived from Tauc plots.[67] Theoretical band gap values (square: $0 \le x_{Al} \le 1$) derived according to eqs 8a−8d by assuming for amorphous oxides the following (see text): χ_{Al} = 1.50; $B_{\eta\text{-}Al2O3}$ = −2.25 eV; $A_{\eta\text{-}Al2O3}$ = 1.67; χ_{Nb} = 1.60; $B_{am\text{-}Nb2O5}$ = −1.35 eV; $A_{am\text{-}Nb2O5}$ = 1.302 (full red squares). Unfilled squares: theoretical band gap values of crystalline anodic films derived as above with $B_{cry\text{-}Nb2O5}$ = −1.50 eV (see text). Optical band gap value (full azure circle) for the polycrystalline $NbAlO_4$ sample.[148]

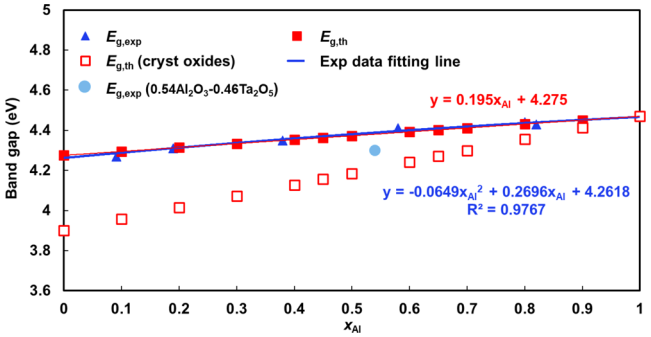

Figure 4. Nondirect optical band gap values vs Al content ($0 \le x_{Al} \le 0.8$) (blue triangles) for amorphous anodic films grown on Al-Ta magnetron-sputtered alloys of various compositions derived from Tauc plots.[43] Theoretical band gap values ($0 \le x_{Al} \le 1$) derived according to eqs 8a−8d by assuming for amorphous oxides the following (see text): χ_{Al} = 1.50; $B_{\eta\text{-}Al2O3}$ = −2.25 eV; $A_{\eta\text{-}Al2O3}$ = 1.67; χ_{Ta} = 1.50; $B_{am\text{-}Ta2O5}$ = −1.125 eV; A_{Ta2O5} = 1.35 (full red squares). Theoretical band gap values of crystalline anodic films (unfilled squares) derived as above with $B_{cry\text{-}Ta2O5}$ = −1.50 eV (see text). Optical band gap value (full azure circle) of a vitreous 54Al_2O_3-46Ta_2O_5 sample.[156]

in the literature.[94,131] These findings suggest that in the case of amorphous alumina, B values equal or lower than that reported in Table 1 for η-Al_2O_3 (−2.25 eV) must be expected.

In Table 1, we reported also possible values of A and B parameters of amorphous alumina (am-Al_2O_3) obtained by using eq 1 and band gap values measured by EELS or optical methods of thin and thick alumina films grown by PVD, spray pyrolysis, or aluminum anodizing in a barrier film, forming electrolytes. For amorphous alumina films grown by the PVD technique (ALD and reactive magnetron sputtering), a rather large range of ρ_{am} values (2.32−3.77 g cm^{-3}) has been reported in the literature[92,94,142−145] as a function of the O/Al ratio, spanning a range of values between 1.30 and 1.72. In the case of amorphous barrier-type anodic alumina obtained by anodizing Al foil, values of ρ between 3.20 and 3.60 g cm^{-3} have been reported.[71,86,92−94,142−145] Owing to the large

https://dx.doi.org/10.1021/acs.inorgchem.0c02691
Inorg. Chem. 2021, 60, 1419−1435

uncertainty in the reported values of the density of alumina anodic film, in the following, values of $B \simeq -2.25$ eV will be assumed to fit the ternary systems involving the presence of amorphous alumina.

Analogous to the widespread range of reported ρ_{am} values, a wide range of experimental values is reported in the literature for amorphous alumina. In fact, E_g values of 5.1−7.1 eV have been reported for thick amorphous alumina films grown by ALD and spray pyrolysis technique.[62,142−144] In some cases, E_g values as low as 3.20−4.30 eV were measured (Tauc plots and EELS methods) for amorphous and ordered alumina very thin films (<2 nm), respectively.[77,146,147]

For anodic passive films grown up to 8 V on Al metal in aqueous solutions of variable pH values ($8 < pH < 14$),[68] band gap values in the range of 3.0−5.0 eV have been measured using the PCS technique. In the absence of direct information on the nature of passivating layers and on the basis of Pourbaix electrochemical equilibria diagrams, the lowest measured band gap (3.0 eV) was attributed to the possible presence of an external amorphous $Al(OH)_3$ phase, while the higher extrapolated E_g values (4.5−5.0 eV) were associated to a less hydrated, possibly oxyhydroxide γ-AlOOH phase. More recently, the anodic photocurrent spectra displaying an indirect band gap value around 4.6 eV were reported in the literature[65] for an as-formed very thin (≃3 nm) alumina film grown up to about 1 V above the equilibrium potential in a quasi-neutral aqueous solution on a pure (99.999%) Al sample. A slight decrease in the measured band gap value (about 4.0 eV) was recorded after longer polarization times at the same anodic potential. The lowering of the band gap could be related to the formation of an external hydrated aluminum oxide (see above), while it is tempting to attribute the highest band gap value initially measured to the possible formation of a defective anhydrous alumina barrier layer having a structure similar to the η-phase described in Peintinger et al.'s work.

In a previous DFT study, E_g values as low as 2.5−3.0 eV have been reported for amorphous alumina;[77] such lower values have been attributed to the underestimation of the band gap usually observed in DFT methods, while the lowering of band gap in amorphous alumina has been associated mainly to a downshift of the conduction band of about 2.5 eV going from crystalline α-Al_2O_3 to am-Al_2O_3. In a recent DFT-based study, Liu et al.[70] have reported a band gap value for amorphous alumina equal to 6.2 eV for a film with a density equal to 3.2 g cm^{-3}, in good agreement with the value reported for an anodic thick film for which a density of 3.3 g cm^{-3} value has been reported.[93] As for thick amorphous barrier-type anodic oxide films grown in aqueous solutions, E_g values around 6.3 eV have been reported in the literature.[68,69]

To further clarify the aspects related to the presence of amorphous alumina units in ternary systems and to highlight the use of eqs 8a−8d in nonregular ternary oxide systems, we will discuss shortly the (sp,d) ternary systems formed by amorphous mixed oxides, $(Nb_{(1-x)}Al_x)_2O_{5-2x}$, $Ta_{(1-x)}Al_x)_2O_{5-2x}$, and $W_{(1-x)}Al_{2x}O_3$, obtained by anodizing Al-Nb, Al-Ta, and Al-W metallic alloys at different compositions. In previous works,[43,66,67] we reported the dependence of $E_{g,opt}$ values of these systems as a function of the starting metal alloy compositions obtained by magnetron cosputtering of pure metals ($x_{Al} \leq 100$ at %). In the following, we will show how previous results pertaining to the ternary s,p-d-metal ternary oxides, challenging the initial correlation, can be now nicely fitted in the frame of the general approach outlined above by using eqs 8a−8d.

3.3.1. Amorphous $(Nb_{(1-x)}Al_x)_2O_{(5-2x)}$. In Figure 3, we report the experimental $E_{g,opt}$ data set points for anodic films grown on Nb-Al magnetron-sputtered alloys[67] from which the following quadratic best fitting equation was obtained

$$E_g = 0.118x_{Al}^2 + 0.8602x_{Al} + 3.3528 \text{ [eV]} \quad (15a)$$

providing a value of 4.33 eV for pure alumina anodic films by extrapolating the $E_{g,opt}$ vs x plot to $x = 1$.

The theoretical fitting points obtained by using eqs 8a−8d are also reported, which thus can be estimated according to the following equation

$$E_{g,th} = 0.1554x_{Al}^2 + 0.8941x_{Al} + 3.3501 \text{ [eV]} \quad (15b)$$

As for η-Al_2O_3, the B value of −2.25 eV and the A value of 1.67 obtained according to eq 1 and by using $E_{g,opt} = 4.40$ eV were used as reported in Table 1. As for amorphous niobia (am-Nb_2O_5), we assumed $\Delta E_{am} = 0.15$ eV obtained as the difference between the optical band gap (3.35 eV) measured for the thick (about 20−30 nm) niobia anodic film and the band gap (3.20 eV) of the crystalline niobia (cr-Nb_2O_5) phase recently reported in the literature for the H-Nb_2O_5 crystalline material.[149,150] According to eq 1, a value of 1.302 is now derived for $A_{H\text{-}Nb2O5}$, which is slightly (−3.2%) lower than the average 1.35 value reported for d-metal oxides. We like to stress, however, that the experimental data could be also fitted by keeping $A = 1.35$ for H-Nb_2O_5 but assuming for χ_{Nb} a value of 1.634, instead of the usual 1.60, still within the uncertainty range of Pauling's scale. It can be noted that a very good fitting of the experimental data is obtained with an EN value of 1.50 for Al and A and B values reported above. The band gap value of 4.40 eV, estimated by Peintinger et al. for η-Al_2O_3, is slightly higher (0.07 eV) than that derived by fitting the experimental data according to eq 15a.

To stress the validity of this new approach, we report also in the same figure the theoretical points (white squares in Figure 3) of the crystalline ternary system derived from the previous ones by assuming $\Delta E_{am} = 0$, i.e., $B_{am} = B_{cryst} = -1.50$ eV, together with the experimental E_g value of 3.63 eV derived from the data reported in the literature[148] for the polycrystalline $AlNbO_4$ sample. This band gap value, as reported by the authors, was obtained by extrapolating linearly to zero the optical absorption spectra of the $AlNbO_4$ sample. A more accurate extrapolation to the constant baseline of the spectrum, in the long-wavelength region, provides a band gap value of 3.71 eV. This last value compares very favorably with the value of 3.76 eV obtained in Figure 3 for the crystalline ternary system of composition $x_{Al} = x_{Nb} = 0.5$. These findings support the initial assumption on the use of η-Al_2O_3 as a partner of amorphous ternary oxides in transition metal aluminates (TM-aluminates), at least as long as the concentration of the TM partner cation remains above a "limiting threshold" of about 20%. The new approach suggests that for Al content up to around 80 at %, the structure of the ternary system am-$(Nb_{(1-x)}Al_x)_2O_{(5-2x)}$ can be imagined as a mixed oxide solid solution where both metallic cations are engaged in structural unities[46,72,132,135] where the bond structure is very similar to that experienced by the same cations in their amorphous (am-Nb_2O_5) or strongly disordered (η-Al_2O_3) structure.

For Al content around 90 at % (or higher), the optical band gap of the ternary oxide reaches values much higher than those

https://dx.doi.org/10.1021/acs.inorgchem.0c02691
Inorg. Chem. 2021, 60, 1419−1435

reported for η-Al_2O_3 (E_g = 4.40 eV). This suggestion is in agreement with the absence of any photocurrent under illumination with photons of 5.3 eV for the oxide film formed on alloy containing 90 at % of Al.[67] It cannot be excluded that at these larger ($x_{Al} \geq 90$ at%) concentrations of Al, a structural modification from η-Al_2O_3 to other polymorphs having a band gap larger than η-Al_2O_3 is occurring. A possible polymorph at very low content of d-metal in the alloys ($x_{TM} < 20$ at %) could be γ-Al_2O_3. In fact, as mentioned above, E_g values around 6.3 ± 0.1 eV, close to the value reported in Table 1, have been attributed to thick (>10 nm) anodic barrier layer alumina films having a short-range order very similar to γ-Al_2O_3.[72]

3.3.2. Amorphous $(Ta_{(1-x)}Al_x)_2O_{(5-2x)}$. The approach previously described for ternary am-$(Nb_{(1-x)}Al_x)_2O_{(5-2x)}$ oxides was employed to fit the experimental data of the optical band gap of amorphous mixed oxides am-$(Ta_{(1-x)}Al_x)_2O_{(5-2x)}$ ($0 \leq x \leq 0.81$) grown on magnetron-sputtered Ta-Al alloys anodized up to 10 V vs Hg/HgO in a borate buffer (pH = 8) solution.[43] The fitting of the experimental data was carried out on a heuristic basis by using the semiempirical correlation previously described for the similar am-$(Nb_{(1-x)}Al_x)_2O_{(5-2x)}$ system.

To fit according to eqs 8a−8d the experimental data, we used now, as starting values, the A and B parameters of d-metal oxides, 1.35 and −1.50 eV, respectively, with χ_{Ta} = 1.50,[34] which provide a band gap value for crystalline Ta_2O_5 (E_{g2}) equal to 3.90 eV. This last value is in very good agreement with the reported band gap values of crystalline orthorhombic β-Ta_2O_5,[151] obtained by thermally annealing the CVD amorphous Ta_2O_5 film in air, as well with an E_g value of 3.95 eV[152] reported for a thicker stabilized anodic oxide film grown on an electropolished (99.9% purity) Ta rod in a 0.5 M H_2SO_4 solution. This value is also in agreement with the band gap value of Ta_2O_5 calculated by DFT techniques with the HSE06 hybrid functional.[153]

To take into account the amorphous nature of anodic films grown on magnetron-sputtered Ta and Ta-Al alloys,[154,155] we assumed a value of ΔE_{am} = 0.375 eV. Such a value accounts, according to eq 14a, for the difference in E_g value between the crystalline Ta_2O_5 (E_g = 3.90 eV) and the larger band gap value (4.275 eV) measured for anodic films grown in a borate buffer solution up to 10 V.[43]

As for the alumina polymorph partner in ternary am-$(Ta_{(1-x)}Al_x)_2O_{(5-2x)}$, a value of E_g = 4.47 eV is obtained by extrapolating to x = 1 the quadratic best fitting line of the experimental data points (see Figure 4)

$$E_g = -0.0649x_{Al}^2 + 0.2696x_{Al} + 4.2618 \text{ [eV]} \quad (16)$$

The theoretical E_g values for the am-$(Ta_{(1-x)}Al_x)_2O_{(5-2x)}$ system were derived by using eqs 8a−8d with the parameters reported in Table 1, slightly modified by the best fitting procedure, for the two pure binary oxides. The theoretical data points were obtained by using for amorphous Ta_2O_5 A = 1.35 and χ_{Ta} = 1.50, together with ΔE_{am} = 0.375 eV, and by assuming A = 1.68, B = −2.25 eV, and χ_{Al} = 1.50 for η-Al_2O_3. Theoretical data points are therefore calculated according to the following equation

$$E_{g,th} = 0.195x_{Al} + 4.275 \quad (17)$$

from which a band gap value of 4.47 eV is derived for a pure alumina film (x = 1). The quadratic and cubic terms in eq 17 are zero (see eqs 8c and 8d) owing to the assumption that $\chi_{Ta} = \chi_{Al}$ = 1.50.

The band gap values of hypothetical ternary cr-$(Ta_{(1-x)}Al_x)_2O_{(5-2x)}$ mixed oxides are also reported (white squares in Figure 4) from which the band gap value of a crystalline $AlTaO_4$ (x = 0.5) phase can be derived. The optical gap value of 4.30 eV pertaining to a vitreous $54Al_2O_3$-$46Ta_2O_5$ sample[156] is about 0.08 eV higher than the corresponding crystalline phase and about 0.08 eV lower than the corresponding amorphous anodic film of equal composition. It seems reasonable to attribute such difference to a different value (0.20 eV) of ΔE_{am} term of this sample owing to the different degree of amorphousness of vitreous Ta_2O_5 ($E_{g,v\text{-}Ta2O5}$ = 4.10 eV) with respect to the anodic film.

Although the general trend of $E_{g,opt}$ vs x_{Al} for Ta-Al anodic films parallels the behavior described above for anodic oxides grown on the Al-Nb system, new features arise when Ta substitutes Nb metal in the sputtered alloys. With respect to the case of Al-Nb alloys, we evidence that a negative bowing coefficient ($b = S_q$ = −0.065) is now derived in the fitting procedure owing to the fact that the measured band gap of anodic oxides show a clear tendency, at higher Al ($x \simeq 0.5$) contents, toward a constant limiting $E_{g,opt}$ value of 4.45 eV very near the theoretical one ($E_{g,th}$ = 4.40 eV) derived for η-Al_2O_3. More importantly, such a limiting value, appearing for Al content around 60 at % for thicker oxide films (≃15 nm), is anticipated to Al content around 40 at % for thinner films (≃8−9 nm) grown up to 5 V vs Hg/HgO under identical conditions (see Figure S3).

As for anodic films grown on Al-Ta alloys, the data of Figure 4 suggest that owing to the smaller difference in the band gap value between am-Ta_2O_5 and η-Al_2O_3, the Al composition range exploitable before the ternary oxide reaches a band gap value equal to that one of η-alumina is now more limited so that for Al content near about 40 at %, in the case of a thinner (5 V) film, or 60 at % for a thicker (10 V) film, the ternary system reaches a band gap value equal to that one of η-alumina.

The data of oxide films grown to 5 and 10 V indicate that such a limiting band gap value, frozen up to around 80 at % of Al content, can be maintained as long as the concentration of the TM cationic partner is sufficient to freeze a disordered lattice structure similar to that of η-alumina. At lower concentration (<10 at %) of the TM cation into the ternary oxide, as mentioned before for the Al-Nb alloy, band gap values larger than that estimated by means of eq 17 are expected owing to the absence of any photocurrent signal under illumination with photons of 5.2 eV. These findings agree with the results reported in the literature[54,157,158] pertaining to aluminates containing small ($x_{TM} \leq 0.1$) amounts of TM cations for which band gap values around 6.1−6.3 eV have been estimated by DFT techniques for mixed ternary oxides α-$Al_{1.875}Nb_{0.125}O$, κ-$Al_{1.875}Nb_{0.125}O_{3.125}$, and α-$Al_{1.8}Ta_{0.2}O_{3.2}$.

Finally, we like to mention that as expected from the generalized approach, a nice fitting of the experimental $E_{g,opt}$ data[136] of anodic films grown on Ta-Nb alloys was observed (see Figure S4) by using for am-$(Nb_{(1-x)}Ta_{x)_2}O_5$ the identical parameters employed for TM oxides in fitting the $E_{g,opt}$ values of ternary oxides grown on Al-Ta and Al-Nb magnetron-sputtered alloys.

3.3.3. Amorphous $(W_{(1-x)}Al_{2x})O_3$. The last system we shall shortly discuss is represented from the ternary am-

https://dx.doi.org/10.1021/acs.inorgchem.0c02691
Inorg. Chem. 2021, 60, 1419−1435

$(W_{(1-x)}Al_{2x})O_3$ anodic films grown on Al-W alloys of various compositions for which a detailed PCS characterization has been reported in a previous work.[66] In Figure 5, the $E_{g,opt}$ values as a function of the Al composition (obtained by RBS analysis)[66] into the mixed oxide film are reported.

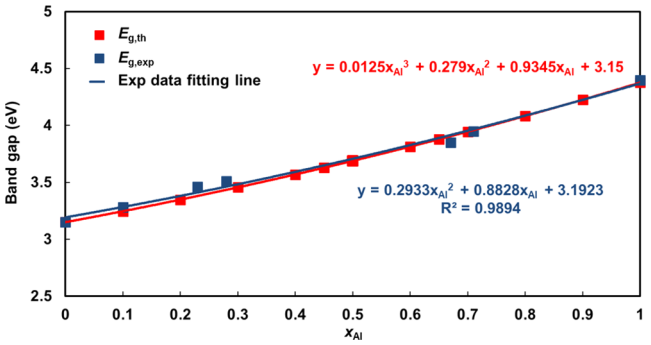

Figure 5. Nondirect optical band gap values vs Al content ($0 \le x_{Al} \le 0.71$) (blue squares) for amorphous anodic films grown on Al-W magnetron-sputtered alloys of various compositions derived from Tauc plots.[66] Theoretical band gap values ($0 \le x_{Al} \le 1$) derived according to eqs 8a–8d by assuming for amorphous oxides the following (see text): $\chi_{Al} = 1.50$; $B_{\eta\text{-}Al2O3} = -2.25$ eV; $A_{\eta\text{-}Al2O3} = 1.68$; $\chi_w = 1.70$; $B_{am\text{-}WO3} = -1.15$ eV ($\Delta E_{am} = 0.35$ eV); $A_{WO3} = 1.35$ (full red squares).

The theoretical fitting points have been obtained by means of eqs 8a–8d by assuming for a-WO_3 a value of $\Delta E_{am} = 0.35$ eV with $\chi_W = 1.70$ and the average values of d-metal oxide for A and B parameters (1.35 and −1.5 eV, respectively). As for η-Al_2O_3, the values reported in Table 1 were used for A (1.667) and B (−2.25 eV), in agreement with the value of $E_g = 4.40$ eV and by assuming an EN value for $\chi_{Al} = 1.50$. For $x_{Al} > 71$ at %, the best fitting parabolic equation provides E_g values between 4.08 eV ($x = 0.8$) and 4.40 eV at variance with the experimental results. In fact, for the concentration of x_W, into the ternary oxide, equal to 21 at %, we were not able to measure any photocurrent as previously noted for Ta-Al and Nb-Al at around the same concentration of TM cations into the films.

The experimental results on all three investigated amorphous ternary systems suggest that when the concentration of the cationic partner decreases below a critical threshold (about 10–20 at %), the η-alumina structure becomes unstable, under anodizing conditions, by changing to a different metastable structure having a larger band gap value. A candidate polymorph could be γ-alumina, which is the more common phase under ordinary conditions and displays a disordered lattice structure used as the starting structure to derive the more disordered η-phase.[52,71,83]

4. CONCLUSIONS

A generalization of the semiempirical approach to the modeling of the band gap of ternary oxides has been carried out, taking into consideration previous criticisms to the limited ability of the initial approach in accounting for the role of oxide polymorphisms in determining the band gap of mixed oxides. We have shown that the influence of the different crystalline structures plays a role in determining the optical band gap of different polymorphs by affecting the two parameters A and B of our semiempirical approach. The B parameter of each polymorph has been assumed to depend on the unit formula volume or density, while the A parameter, derived by means of the initial correlation between the band gap and difference in electronegativity between oxygen and average cationic electronegativity, changes owing to changes in the average strength of the oxygen–metal bond.

A re-examination of experimental data of pseudoregular (sp,sp mixed oxides) and nonregular (sp,d mixed oxides) systems seems to validate the proposed generalization of our semiempirical model. The investigated systems allowed also one to test the proposed generalization in a rather large range of band gap values as those reported for alumina polymorphs by including also the metastable η-Al_2O_3 polymorph for which the proposed band gap value of E_g (4.4 eV) derived by DFT techniques was used to fit the band gap dependence, E_g vs x_{Al} at %, of amorphous mixed oxides grown on Al-TM (Nb, Ta, and W) alloys of various compositions. From the study of these last amorphous systems, it shows that a minimum concentration threshold of the TM cation, in the order of 20 at % into the oxide, seems necessary to keep a short-range order between Al^{3+} cations and O^{2-} anions similar to that reported for η-Al_2O_3. The concentration threshold of the TM cation is quite near the percolation threshold foreseen for the formation of a delocalized distribution of electronic states (formation of a conduction band) in random distributed $Ni_xMg_{(1-x)}$ O mixed oxide.[140]

At lower TM cation concentration (around 10 at %), a deviation from the theoretical fitting line was observed in all amorphous nonregular ternary systems investigated, probably owing to the formation of a mixed ternary oxide having a different short-range order between Al^{3+} and O^{2-} anions, more similar to that reported for other metastable alumina phases of a larger band gap doped with a very low (<10 at %) concentration of TM ions.[54,157,158] In our case, the formation of amorphous mixed ternary oxides with short-range order Al-O between Al^{3+} and O^{2-} anions similar to β,γ-Al_2O_3 seems reasonable and is in agreement with the photocurrent spectroscopy experimental findings. Further studies on these aspects could be very useful for the possible use of these mixed oxides in the field of high-k materials. Although only three alumina polymorphs were involved in this work, it will be shown in a future paper how other alumina polymorphs have to be used for fitting the optical band gap values of different crystalline alumina-TM ternary and quaternary oxides.

■ ASSOCIATED CONTENT

Supporting Information

The Supporting Information is available free of charge at https://pubs.acs.org/doi/10.1021/acs.inorgchem.0c02691.

Fitting of all experimental data sets of β-$((Ga_{(1-x)}Al_x)_2O_3)$ band gap values (Figure S1); discussion and fitting of β-$((Ga_{(1-x)}Al_x)_2O_3)$ direct optical band gap values (Figure S2); fitting of E_g vs x_{Al} for Al-Ta mixed oxide thin films (Figure S3); fitting of $E_{g,opt}$ values for Nb-Ta mixed oxide values (Figure S4); fitting parameters for the different Al-(Ga, Nb, Ta, W) oxide systems studied (Table S1) (PDF)

■ AUTHOR INFORMATION

Corresponding Author

Francesco Di Quarto − *Dipartimento di Ingegneria, Università degli Studi di Palermo, 90128 Palermo, Italy;* orcid.org/0000-0001-8751-5928;

https://dx.doi.org/10.1021/acs.inorgchem.0c02691
Inorg. Chem. 2021, 60, 1419–1435

Phone: +393204328592; Email: francesco.diquarto@unipa.it

Authors

Andrea Zaffora − *Dipartimento di Ingegneria, Università degli Studi di Palermo, 90128 Palermo, Italy;* orcid.org/0000-0002-4185-8308

Francesco Di Franco − *Dipartimento di Ingegneria, Università degli Studi di Palermo, 90128 Palermo, Italy;* orcid.org/0000-0002-5722-2881

Monica Santamaria − *Dipartimento di Ingegneria, Università degli Studi di Palermo, 90128 Palermo, Italy*

Complete contact information is available at: https://pubs.acs.org/10.1021/acs.inorgchem.0c02691

Notes

The authors declare no competing financial interest.

■ ACKNOWLEDGMENTS

The authors thank Mrs. Maria Rita Cinà for her support in providing many of the articles cited in References section.

■ REFERENCES

(1) Gerosa, M.; Bottani, C. E.; Di Valentin, C.; Onida, G.; Pacchioni, G. Accuracy of Dielectric-Dependent Hybrid Functionals in the Prediction of Optoelectronic Properties of Metal Oxide Semiconductors: A Comprehensive Comparison with Many-Body GW and Experiments. *J. Phys. Condens. Matter* **2018**, *30*, No. 044003.

(2) Zaffora, A.; Di Quarto, F.; Kura, C.; Sato, Y.; Aoki, Y.; Habazaki, H.; Santamaria, M. Electrochemical Oxidation of Hf-Nb Alloys as a Valuable Route to Prepare Mixed Oxides of Tailored Dielectric Properties. *Adv. Electron. Mater.* **2018**, *4*, 1800006.

(3) Robertson, J.; Wallace, R. M. High-K Materials and Metal Gates for CMOS Applications. *Mater. Sci. Eng.: R: Rep.* **2015**, *88*, 1−41.

(4) Zaffora, A.; Di Quarto, F.; Habazaki, H.; Valov, I.; Santamaria, M. Electrochemically Prepared Oxides for Resistive Switching Memories. *Faraday Discuss.* **2019**, *213*, 165−181.

(5) Ohko, Y.; Saitoh, S.; Tatsuma, T.; Fujishima, A. Photoelectrochemical Anticorrosion and Self-Cleaning Effects of a TiO_2 Coating for Type 304 Stainless Steel. *J. Electrochem. Soc.* **2001**, *148*, B24.

(6) Di Franco, F.; Zaffora, A.; Santamaria, M.; Di Quarto, F. Anodization and Anodic Oxides. In *Encyclopedia of Interfacial Chemistry: Surface Science and Electrochemistry*; Wandelt, K., Ed.; Elsevier: Waltham, MA, 2018; pp. 26−40.

(7) Zaffora, A.; Macaluso, R.; Habazaki, H.; Valov, I.; Santamaria, M. Electrochemically Prepared Oxides for Resistive Switching Devices. *Electrochim. Acta* **2018**, *274*, 103−111.

(8) Medvedev, M. G.; Bushmarinov, I. S.; Sun, J.; Perdew, J. P.; Lyssenko, K. A. Density Functional Theory Is Straying from the Path toward the Exact Functional. *Science* **2017**, *355*, 49−52.

(9) Garza, A. J.; Scuseria, G. E. Predicting Band Gaps with Hybrid Density Functionals. *J. Phys. Chem. Lett.* **2016**, *7*, 4165−4170.

(10) Ma, J.; Wang, L.-W. Using Wannier Functions to Improve Solid Band Gap Predictions in Density Functional Theory. *Sci. Rep.* **2016**, *6*, 24924.

(11) Perdew, J. P.; Yang, W.; Burke, K.; Yang, Z.; Gross, E. K. U.; Scheffler, M.; Scuseria, G. E.; Henderson, T. M.; Zhang, I. Y.; Ruzsinszky, A.; et al. Understanding Band Gaps of Solids in Generalized Kohn-Sham Theory. *Proc. Natl. Acad. Sci.* **2017**, *114*, 2801−2806.

(12) Tran, F.; Blaha, P. Importance of the Kinetic Energy Density for Band Gap Calculations in Solids with Density Functional Theory. *J. Phys. Chem. A* **2017**, *121*, 3318−3325.

(13) Contreras-García, J.; Cardenas, C. On Understanding the Chemical Origin of Band Gaps. *J. Mol. Model.* **2017**, *23*, 271.

(14) Morales-García, Á.; Valero, R.; Illas, F. An Empirical, yet Practical Way to Predict the Band Gap in Solids by Using Density Functional Band Structure Calculations. *J. Phys. Chem. C* **2017**, *121*, 18862−18866.

(15) Tran, F.; Ehsan, S.; Blaha, P. Assessment of the GLLB-SC Potential for Solid-State Properties and Attempts for Improvement. *Phys. Rev. Mater.* **2018**, No. 023802.

(16) Suram, S. K.; Newhouse, P. F.; Gregoire, J. M. High Throughput Light Absorber Discovery, Part 1: An Algorithm for Automated Tauc Analysis. *ACS Comb. Sci.* **2016**, *18*, 673−681.

(17) Suram, S. K.; Newhouse, P. F.; Zhou, L.; Van Campen, D. G.; Mehta, A.; Gregoire, J. M. High Throughput Light Absorber Discovery, Part 2: Establishing Structure-Band Gap Energy Relationships. *ACS Comb. Sci.* **2016**, *18*, 682−688.

(18) Dolgonos, A.; Mason, T. O.; Poeppelmeier, K. R. Direct Optical Band Gap Measurement in Polycrystalline Semiconductors: A Critical Look at the Tauc Method. *J. Solid State Chem.* **2016**, *240*, 43−48.

(19) Schwarting, M.; Siol, S.; Talley, K.; Zakutayev, A.; Phillips, C. Automated Algorithms for Band Gap Analysis from Optical Absorption Spectra. *Mater. Discovery* **2017**, *10*, 43−52.

(20) Sharp, D. J.; Panitz, J. K. G.; Merrill, R. M.; Haaland, D. M. The Incorporation of Electrolyte Byproducts into Barrier Anodic Al_2O_3 Coatings. *Thin Solid Films* **1984**, *111*, 227−234.

(21) Shimizu, K.; Kobayashi, K.; Thompson, G. E.; Skeldon, P.; Wood, G. C. Anodic Oxide Films on Tantalum: Incorporation and Mobilities of Electrolyte-Derived Species. *Philos. Mag. B* **1996**, *73*, 461−485.

(22) Di Franco, F.; Santamaria, M.; Di Quarto, F.; Tsuji, E.; Habazaki, H. The Influence of Nitrogen Incorporation on the Optical Properties of Anodic Ta_2O_5. *Electrochim. Acta* **2012**, *59*, 382−386.

(23) Zaffora, A.; Santamaria, M.; Di Franco, F.; Habazaki, H.; Di Quarto, F. Photoelectrochemical Evidence of Inhomogeneous Composition at Nm Length Scale of Anodic Films on Valve Metals Alloys. *Electrochim. Acta* **2016**, *201*, 333−339.

(24) Di Franco, F.; Zaffora, A.; Santamaria, M. Band Gap Narrowing and Dielectric Constant Enhancement of $(Nb_xTa_{(1-x)})_2O_5$ by Electrochemical Nitrogen Doping. *Electrochim. Acta* **2018**, *265*, 326−335.

(25) Zaffora, A.; Di Franco, F.; Di Quarto, F.; Santamaria, M. Optimization of Anodizing Process of Tantalum for Ta_2O_5-Based Capacitors. *J. Solid State Electrochem.* **2020**, 2953.

(26) Miraghaei, S.; Santamaria, M.; Di Quarto, F. Red Shift in the Light Absorption Threshold of Anodic TiO_2 Films Induced by Nitrogen Incorporation. *Electrochim. Acta* **2014**, *134*, 150−158.

(27) Di Quarto, F.; Sunseri, C.; Piazza, S.; Romano, M. C. Semiempirical Correlation between Optical Band Gap Values of Oxides and the Difference of Electronegativity of the Elements. Its Importance for a Quantitative Use of Photocurrent Spectroscopy in Corrosion Studies. *J. Phys. Chem. B* **1997**, *101*, 2519−2525.

(28) Di Quarto, F.; Santamaria, M. Semiempirical Correlation Between Optical Bandgap and Electronegativities in Group III Nitride Alloys. *Electrochem. Solid-State Lett.* **2008**, *11*, H313−H315.

(29) Di Quarto, F.; Santamaria, M.; Sunseri, C. Photoelectrochemical Techniques in Corrosion Studies. In *Analytical Methods in Corrosion Science and Technology*; Marcus, P., Mansfeld, F., Eds.; Taylor & Francis Group: Boca Raton, 2005; pp. 697−732.

(30) Di Quarto, F.; La Mantia, F.; Santamaria, M. Physicochemical Characterization of Passive Films and Corrosion Layers by Differential Admittance and Photocurrent Spectroscopy. In *Modern Aspects of Electrochemistry, No. 46: Progress in Corrosion Science and Engineering I*; Pyun, S.-I., Lee, J.-W., Eds.; Springer: New York, 2009; pp. 231−316.

(31) Di Quarto, F.; Di Franco, F.; Zaffora, A.; Santamaria, M. Photocurrent Spectroscopy in Passivity Studies. In *Encyclopedia of Interfacial Chemistry: Surface Science and Electrochemistry*; Wandelt, K., Ed.; 2018; Vol. *1*, pp. 361−371.

(32) Di Quarto, F.; Zaffora, A.; Di Franco, F.; Santamaria, M. Critical Review—Photocurrent Spectroscopy in Corrosion and

Passivity Studies: A Critical Assessment of the Use of Band Gap Value to Estimate the Oxide Film Composition. *J. Electrochem. Soc.* **2017**, *164*, C671−C681.
(33) Walsh, A.; Butler, K. T. Prediction of Electron Energies in Metal Oxides. *Acc. Chem. Res.* **2014**, *47*, 364−372.
(34) Pauling, L. *The Nature of Chemical Bond*; Cornell University Press: Ithaca, New York, 1959.
(35) Pearton, S. J.; Yang, J.; Cary, P. H., IV; Ren, F.; Kim, J.; Tadjer, M. J.; Mastro, M. A. A Review of Ga_2O_3 Materials, Processing, and Devices. *Appl. Phys. Rev.* **2018**, *5*, No. 011301.
(36) Chen, X.; Ren, F.; Gu, S.; Ye, J. Review of Gallium-Oxide-Based Solar-Blind Ultraviolet Photodetectors. *Photonics Res.* **2019**, *7*, 381−415.
(37) Feng, Q.; Li, X.; Han, G.; Huang, L.; Li, F.; Tang, W.; Zhang, J.; Hao, Y. $(AlGa)_2O_3$ Solar-Blind Photodetectors on Sapphire with Wider Bandgap and Improved Responsivity. *Opt. Mater. Express* **2017**, *7*, 1240−1248.
(38) Feng, Q.; Hu, Z.; Feng, Z.; Xing, X.; Zuo, Y.; Yan, G.; Lu, X.; Zhang, C.; Zhou, H.; Zhang, J. Research on the Growth of β-$(AlGa)_2O_3$ Film and the Analysis of Electrical Characteristics of Ni/Au Schottky Contact Using Tung's Model. *Superlattices Microstruct.* **2018**, *120*, 441−447.
(39) Lee, H.; Liu, J.; Lee, C. Modulated Al_2O_3 -Alloyed Ga_2O_3 Materials and Deep Ultraviolet Photodetectors. *IEEE Photonics Technol. Lett.* **2018**, *30*, 2018−2021.
(40) Kamada, K.; Endo, T.; Tsutumi, K.; Yanagida, T.; Fujimoto, Y.; Fukabori, A.; Yoshikawa, A.; Pejchal, J.; Nikl, M. Composition Engineering in Cerium-Doped $(Lu,Gd)_3(Ga,Al)_5O_{12}$ Single-Crystal Scintillators. *Cryst. Growth Des.* **2011**, *11*, 4484−4490.
(41) Vrubel, I. I.; Polozkov, R. G.; Shelykh, I. A.; Khanin, V. M.; Rodnyi, P. A.; Ronda, C. R. Bandgap Engineering in Yttrium-Aluminum Garnet with Ga Doping. *Cryst. Growth Des.* **2017**, *17*, 1863−1869.
(42) Ueda, J.; Tanabe, S. Review of Luminescent Properties of Ce^{3+}-Doped Garnet Phosphors: New Insight into the Effect of Crystal and Electronic Structure. *Opt. Mater. X* **2019**, *1*, 100018.
(43) Zaffora, A.; Di Franco, F.; Santamaria, M.; Habazaki, H.; Di Quarto, F. The Influence of Composition on Band Gap and Dielectric Constant of Anodic Al-Ta Mixed Oxides. *Electrochim. Acta* **2015**, *180*, 666−678.
(44) Amato, A.; Terreni, S.; Granata, M.; Michel, C.; Sassolas, B.; Pinard, L.; Canepa, M.; Cagnoli, G. Observation of a Correlation Between Internal Friction and Urbach Energy in Amorphous Oxides Thin Films. *Sci. Rep.* **2020**, *10*, 1670.
(45) Shyam, B.; Stone, K. H.; Bassiri, R.; Fejer, M. M.; Toney, M. F.; Mehta, A. Measurement and Modeling of Short and Medium Range Order in Amorphous Ta_2O_5 Thin Films. *Sci. Rep.* **2016**, *6*, 32170.
(46) Bassiri, R.; Abernathy, M. R.; Liou, F.; Mehta, A.; Gustafson, E. K.; Hart, M. J.; Isa, H. N.; Kim, N.; Lin, A. C.; Maclaren, I.; et al. Order, Disorder and Mixing: The Atomic Structure of Amorphous Mixtures of Titania and Tantala. *J. Non-Cryst. Solids* **2016**, *438*, 59−66.
(47) Amato, A.; Terreni, S.; Granata, M.; Michel, C.; Pinard, L.; Gemme, G.; Canepa, M.; Cagnoli, G. Effect of Heating Treatment and Mixture on Optical Properties of Coating Materials Used in Gravitational-Wave Detectors. *J. Vac. Sci. Technol., B* **2019**, *37*, No. 062913.
(48) Kim, N.; Stebbins, J. F. Structure of Amorphous Tantalum Oxide and Titania-Doped Tantala: ^{17}O NMR Results for Sol-Gel and Ion-Beam-Sputtered Materials. *Chem. Mater.* **2011**, *23*, 3460−3465.
(49) Phillips, J. C. *Bonds and Bands in Semiconductors*; Academic Press: New York, London, 1973.
(50) Alonso, J. A.; March, N. H. *Electrons in Metals and Alloys*; Academic Press: New York, London, 1989.
(51) Batsanov, S. S.; Batsanov, A. S. *Introduction to Structural Chemistry*; p. 90, Springer: 2012; DOI: 10.1007/978-94-007-4771-5.
(52) Peintinger, M. F.; Kratz, M. J.; Bredow, T. Quantum-Chemical Study of Stable, Meta-Stable and High-Pressure Alumina Polymorphs and Aluminum Hydroxides. *J. Mater. Chem. A* **2014**, *2*, 13143−13158.
(53) Olivier, J.; Poirier, R. Electronic Structure of Al_2O_3 from Electron Energy Loss Spectroscopy. *Surf. Sci.* **1981**, *105*, 347−356.
(54) Haverty, M.; Kawamoto, A.; Cho, K.; Dutton, R. First-Principles Study of Transition-Metal Aluminates as High-*k* Gate Dielectrics. *Appl. Phys. Lett.* **2002**, *80*, 2669−2671.
(55) Wallin, E.; Andersson, J. M.; Chirita, V.; Helmersson, U. Effects of Additives in α- and θ-Alumina: An *Ab Initio* Study. *J. Phys. Condens. Matter* **2004**, *16*, 8971−8980.
(56) Hattori, M.; Oshima, T.; Wakabayashi, R.; Yoshimatsu, K.; Sasaki, K.; Masui, T.; Kuramata, A.; Yamakoshi, S.; Horiba, K.; Kumigashira, H.; et al. Epitaxial Growth and Electric Properties of γ-$Al_2O_3(110)$ Films on β-$Ga_2O_3(010)$ Substrates. In *Japanese Journal of Applied Physics*; Japan Society of Applied Physics: 2016; Vol. *55*, p 1202B6.
(57) Casillas, J. E.; Campa-Molina, J.; Tzompantzi, F.; Carbajal Arízaga, G. G.; López-Gaona, A.; Ulloa-Godínez, S.; Cano, M. E.; Barrera, A. Photocatalytic Degradation of Diclofenac Using Al_2O_3-Nd_2O_3 Binary Oxides Prepared by the Sol-Gel Method. *Materials* **2020**, *13*, 1345.
(58) Oshima, T.; Kato, Y.; Kobayashi, E.; Takahashi, K. Measurements of the Band Alignment at Coherent A-Ga_2O_3/Al_2O_3 Heterojunctions. *Jpn. J. Appl. Phys.* **2018**, *57*, No. 080308.
(59) Ching, W. Y.; Ouyang, L.; Rulis, P.; Yao, H. *Ab Initio* Study of the Physical Properties of γ-Al_2O_3: Lattice Dynamics, Bulk Properties, Electronic Structure, Bonding, Optical Properties, and ELNES/XANES Spectra. *Phys. Rev. B* **2008**, *78*, No. 014106.
(60) Aryal, S.; Rulis, P.; Ouyang, L.; Ching, W. Y. Structure and Properties of the Low-Density Phase ι-Al_2O_3 from First Principles. *Phys. Rev. B* **2011**, *84*, 174123.
(61) Lee, C. K.; Cho, E.; Lee, H. S.; Seol, K. S.; Han, S. Comparative Study of Electronic Structures and Dielectric Properties of Alumina Polymorphs by First-Principles Methods. *Phys. Rev. B* **2007**, *76*, 245110.
(62) French, B. L.; King, S. W. Detection of Surface Electronic Defect States in Low and High-k Dielectrics Using Reflection Electron Energy Loss Spectroscopy. *J. Mater. Res.* **2013**, *28*, 2771−2784.
(63) Filatova, E. O.; Konashuk, A. S. Interpretation of the Changing the Band Gap of Al_2O_3 Depending on Its Crystalline Form: Connection with Different Local Symmetries. *J. Phys. Chem. C* **2015**, *119*, 20755−20761.
(64) Tahir, D.; Kwon, H. L.; Shin, H. C.; Oh, S. K.; Kang, H. J.; Heo, S.; Chung, J. G.; Lee, J. C.; Tougaard, S. Electronic and Optical Properties of Al_2O_3/SiO_2 Thin Films Grown on Si Substrate. *J. Phys. D: Appl. Phys.* **2010**, *43*, 255301.
(65) Ura-Binczyk, E.; Beni, A.; Lewandowska, M.; Schmutz, P. Passive Oxide Film Characterisation on Al-Cr-Fe and Al-Cu-Fe-Cr Complex Metallic Alloys in Neutral to Alkaline Electrolytes by Photo- and Electrochemical Methods. *Electrochim. Acta* **2014**, *139*, 289−301.
(66) Piazza, S.; Santamaria, M.; Sunseri, C.; Di Quarto, F. Recent Advances in Photocurrent Spectroscopy of Passive Films. *Electrochim. Acta* **2003**, *48*, 1105−1114.
(67) Santamaria, M.; Di Franco, F.; Di Quarto, F.; Skeldon, P.; Thompson, G. E. Tailoring of the Solid State Properties of Al−Nb Mixed Oxides: A Photoelectrochemical Study. *J. Phys. Chem. C* **2013**, *117*, 4201−4210.
(68) Tuccio, G.; Piazza, S.; Sunseri, C.; Di Quarto, F. Effect of the Initial Treatment on the Structure of Thin Anodic Films on Aluminum. *J. Electrochem. Soc.* **1999**, *146*, 493−501.
(69) Di Quarto, F.; Piazza, S.; Splendore, A.; Sunseri, C. More Insights on the Photocurrent Behavior of the Aluminum/Aluminum Oxide/Electrolyte Junction. In *Proceedings of the Symposium on Oxide Films on Metals and Alloys*; MacDougall, B. R., Alwitt, R. S., Ramanarayanan, T. A., Eds.; The Electrochemical Society Inc.: Pennington, N.J., 1992; pp. 311−325.
(70) Liu, D.; Guo, Y.; Lin, L.; Robertson, J. First-Principles Calculations of the Electronic Structure and Defects of Al_2O_3. *J. Appl. Phys.* **2013**, *114*, No. 083704.

(71) Levin, I.; Brandon, D. Metastable Alumina Polymorphs: Crystal Structures and Transition Sequences. *J. Am. Ceram. Soc.* **1998**, *81*, 1995−2012.
(72) Shimizu, K.; Kobayashi, K.; Thompson, G. E.; Wood, G. C. High-Resolution and Cross-Sectional Transmission Electron Microscopy for Oxidation Studies of Metals and Alloys. In *Proceedings of the Symposium on Oxide Films on Metals and Alloys*; MacDougall, B. R., Alwitt, R. S., Ramanarayanan, T. A., Eds.; The Electrochemical Society Inc.: 1992; pp 92, 23−38.
(73) Ito, H.; Kaneko, K.; Fujita, S. Growth and Band Gap Control of Corundum-Structured α-$(AlGa)_2O_3$ Thin Films on Sapphire by Spray-Assisted Mist Chemical Vapor Deposition. *Jpn. J. Appl. Phys.* **2012**, *51*, 100207.
(74) Krueger, B. W.; Dandeneau, C. S.; Nelson, E. M.; Dunham, S. T.; Ohuchi, F. S.; Olmstead, M. A. Variation of Band Gap and Lattice Parameters of B−$(Al_xGa_{1-x})_2O_3$ Powder Produced by Solution Combustion Synthesis. *J. Am. Ceram. Soc.* **2016**, *99*, 2467−2473.
(75) Furthmüller, J.; Bechstedt, F. Quasiparticle Bands and Spectra of Ga_2O_3 Polymorphs. *Phys. Rev. B* **2016**, *93*, 115204.
(76) Glasser, L. Solid-State Energetics and Electrostatics: Madelung Constants and Madelung Energies. *Inorg. Chem.* **2012**, *51*, 2420−2424.
(77) Århammar, C.; Pietzsch, A.; Bock, N.; Holmström, E.; Araujo, C. M.; Gråsjö, J.; Zhao, S.; Green, S.; Peery, T.; Hennies, F.; et al. Unveiling the Complex Electronic Structure of Amorphous Metal Oxides. *Proc. Natl. Acad. Sci. U. S. A.* **2011**, *108*, 6355−6360.
(78) Kirm, M.; Feldbach, E.; Kotlov, A.; Liblik, P.; Lushchik, A.; Oja, M.; Palcevskis, E. VUV Spectroscopy and Electronic Excitations in Nano-Size Alumina. *Radiat. Meas.* **2010**, *45*, 618−620.
(79) Yourdshahyan, Y.; Ruberto, C.; Halvarsson, M.; Bengtsson, L.; Langer, V.; Lundqvist, B. I.; Ruppi, S.; Rolander, U. Theoretical Structure Determination of a Complex Material: κ-Al2O3. *J. Am. Ceram. Soc.* **2004**, *82*, 1365−1380.
(80) Ito, K.; Kikuta, D.; Narita, T.; Kataoka, K.; Isomura, N.; Kitazumi, K.; Mori, T. Band Offset of Al1-XSixOy Mixed Oxide on GaN Evaluated by Hard X-Ray Photoelectron Spectroscopy. In *Japanese Journal of Applied Physics*; Japan Society of Applied Physics: 2017; Vol. 56, p 04CG07.
(81) Carey, P. H., IV; Ren, F.; Hays, D. C.; Gila, B. P.; Pearton, S. J.; Jang, S.; Kuramata, A. Band Alignment of Al_2O_3 with (−201) β-Ga_2O_3. *Vacuum* **2017**, *142*, 52−57.
(82) Franchy, R.; Schmitz, G.; Gassmann, P.; Bartolucci, F. Growth of Thin, Crystalline Oxide, Nitride, and Oxynitride Films on NiAl and CoGa Surfaces. *Appl. Phys. A: Mater. Sci. Process.* **1997**, *65*, 551−566.
(83) Zhou, R.-S.; Snyder, R. L. Structures and Transformation Mechanisms of the η, γ and θ Transition Aluminas. *Acta Crystallogr., Sect. B: Structural Science* **1991**, *47*, 617−630.
(84) Krokidis, X.; Raybaud, P.; Gobichon, A. E.; Rebours, B.; Euzen, P.; Toulhoat, H. Theoretical Study of the Dehydration Process of Boehmite to γ-Alumina. *J. Phys. Chem. B* **2001**, *105*, 5121−5130.
(85) Oshima, T.; Kato, Y.; Oda, M.; Hitora, T.; Kasu, M. Epitaxial Growth of γ-$(Al_xGa_{1-x})O_3$ Alloy Films for Band-Gap Engineering. *Appl. Phys. Express* **2017**, *10*, No. 051104.
(86) Evangelisti, F.; Stiefel, M.; Guseva, O.; Partovi Nia, R.; Hauert, R.; Hack, E.; Jeurgens, L. P. H.; Ambrosio, F.; Pasquarello, A.; Schmutz, P.; et al. Electronic and Structural Characterization of Barrier-Type Amorphous Aluminium Oxide. *Electrochim. Acta* **2017**, *224*, 503−516.
(87) Kijima, Y.; Hanada, T. Effect of the Pressure of Sputtering Atmosphere on the Physical Properties of Amorphous Aluminum Oxide Films. *J. Mater. Sci.* **2000**, *35*, 2193−2199.
(88) Cai, S. H.; Rashkeev, S. N.; Pantelides, S. T.; Sohlberg, K. Phase Transformation Mechanism between γ- and θ-Alumina. *Phys. Rev.* **2003**, *67*, 224104.
(89) Bender, H.; Conard, T.; Nohira, H.; Petry, J.; Richard, O.; Zhao, C.; Brijs, B.; Besling, W.; Detavernier, C.; Vandervorst, W. et al. Physical Characterisation of High-k Gate Stacks Deposited on HF-Last Surfaces. In *Extended Abstracts of International Workshop on Gate Insulator, IWGI 2001*; Institute of Electrical and Electronics Engineers Inc.: 2001; pp. 86−92.
(90) Adamopoulos, G.; Thomas, S.; Bradley, D. D. C.; McLachlan, M. A.; Anthopoulos, T. D. Low-Voltage ZnO Thin-Film Transistors Based on Y_2O_3 and Al_2O_3 High-k Dielectrics Deposited by Spray Pyrolysis in Air. *Appl. Phys. Lett.* **2011**, *98*, 123503.
(91) Riffet, V.; Vidal, J. Statistics-Based Analysis of the Evolution of Structural and Electronic Properties of Realistic Amorphous Alumina during the Densification Process: Insights from First-Principles Approach. *J. Phys. Chem. C* **2017**, *121*, 24745−24758.
(92) Koski, K.; Hölsä, J.; Juliet, P. Properties of Aluminium Oxide Thin Films Deposited by Reactive Magnetron Sputtering. *Thin Solid Films* **1999**, *339*, 240−248.
(93) Skeldon, P.; Shimizu, K.; Thompson, G. E.; Wood, G. C. Barrier-Type Anodic Films on Aluminium in Aqueous Borate Solutions: 1-Film Density and Stopping Power of Anodic Alumina Films for Alpha Particles. *Surf. Interface Anal.* **1983**, *5*, 247−251.
(94) Gutiérrez, G.; Johansson, B. Molecular Dynamics Study of Structural Properties of Amorphous Al_2O_3. *Phys. Rev. B* **2002**, *65*, 104202.
(95) Dawson, J. A.; Robertson, J. Nature of Cu Interstitials in Al_2O_3 and the Implications for Filament Formation in Conductive Bridge Random Access Memory Devices. *J. Phys. Chem. C* **2016**, *120*, 14474−14483.
(96) Shinohara, D.; Fujita, S. Heteroepitaxy of Corundum-Structured α-Ga_2O_3 Thin Films on α-Al_2O_3 Substrates by Ultrasonic Mist Chemical Vapor Deposition. *Jpn. J. Appl. Phys.* **2008**, *47*, 7311−7313.
(97) von Wenckstern, H. Group-III Sesquioxides: Growth, Physical Properties and Devices. *Adv. Electron. Mater.* **2017**, *3*, 1600350.
(98) Wang, T.; Li, W.; Ni, C.; Janotti, A. Band Gap and Band Offset of Ga_2O_3 and $(Al_xGa_{1-x})_2O_3$ Alloys. *Phys. Rev. Appl.* **2018**, *10*, No. 011003.
(99) Peelaers, H.; Varley, J. B.; Speck, J. S.; Van De Walle, C. G. Structural and Electronic Properties of Ga_2O_3-Al_2O_3 Alloys. *Appl. Phys. Lett.* **2018**, *112*, 242101.
(100) Yao, Y.; Okur, S.; Lyle, L. A. M.; Tompa, G. S.; Salagaj, T.; Sbrockey, N.; Davis, R. F.; Porter, L. M. Growth and Characterization of α-, β-, and ϵ-Phases of Ga_2O_3 Using MOCVD and HVPE Techniques. *Mater. Res. Lett.* **2018**, *6*, 268−275.
(101) Schmidt-Grund, R.; Kranert, C.; Von Wenckstern, H.; Zviagin, V.; Lorenz, M.; Grundmann, M. Dielectric Function in the Spectral Range (0.5-8.5)EV of an $(AlxGa_{1-x})_2O_3$ Thin Film with Continuous Composition Spread. *J. Appl. Phys.* **2015**, *117*, 165307.
(102) Sun, H.; Li, K. H.; Castanedo, C. G. T.; Okur, S.; Tompa, G. S.; Salagaj, T.; Lopatin, S.; Genovese, A.; Li, X. HCl Flow-Induced Phase Change of α-, β-, and ϵ-Ga_2O_3 Films Grown by MOCVD. *Cryst. Growth Des.* **2018**, *18*, 2370−2376.
(103) Oshima, Y.; Víllora, E. G.; Matsushita, Y.; Yamamoto, S.; Shimamura, K. Epitaxial Growth of Phase-Pure ϵ-Ga_2O_3 by Halide Vapor Phase Epitaxy. *J. Appl. Phys.* **2015**, *118*, No. 085301.
(104) Kneiß, M.; Hassa, A.; Splith, D.; Sturm, C.; Von Wenckstern, H.; Schultz, T.; Koch, N.; Lorenz, M.; Grundmann, M. Tin-Assisted Heteroepitaxial PLD-Growth of κ-Ga_2O_3 Thin Films with High Crystalline Quality. *APL Mater.* **2019**, *7*, No. 022516.
(105) Hinuma, Y.; Gake, T.; Oba, F. Band Alignment at Surfaces and Heterointerfaces of Al_2O_3, Ga_2O_3, In_2O_3, and Related Group-III Oxide Polymorphs: A First-Principles Study. *Phys. Rev. Mater.* **2019**, *3*, No. 084605.
(106) French, R. H. Electronic Band Structure of Al_2O_3, with Comparison to Alon and AIN. *J. Am. Ceram. Soc.* **1990**, *73*, 477−489.
(107) Peelaers, H.; Varley, J. B.; Speck, J. S.; Van De Walle, C. G. Erratum: "Structural and Electronic Properties of Ga_2O_3-Al_2O_3 Alloys" [Appl. Phys. Lett. 112, 242101 (2018)]. *Appl. Phys. Lett.* **2019**, *115*, 159901.
(108) Chikoidze, E.; Von Bardeleben, H. J.; Akaiwa, K.; Shigematsu, E.; Kaneko, K.; Fujita, S.; Dumont, Y. Electrical, Optical, and Magnetic Properties of Sn Doped α-Ga_2O_3 Thin Films. *J. Appl. Phys.* **2016**, *120*, No. 025109.

https://dx.doi.org/10.1021/acs.inorgchem.0c02691
Inorg. Chem. 2021, 60, 1419−1435

(109) Segura, A.; Artús, L.; Cuscó, R.; Goldhahn, R.; Feneberg, M. Band Gap of Corundumlike α-Ga_2O_3 Determined by Absorption and Ellipsometry. *Phys. Rev. Mater.* **2017**, *1*, No. 024604.
(110) Nishinaka, H.; Tahara, D.; Morimoto, S.; Yoshimoto, M. Epitaxial Growth of α-Ga_2O_3 Thin Films on a-, m-, and r-Plane Sapphire Substrates by Mist Chemical Vapor Deposition Using α-Fe_2O_3 Buffer Layers. *Mater. Lett.* **2017**, *205*, 28−31.
(111) Matsumoto, T.; Aoki, M.; Kinoshita, A.; Aono, T. Absorption and Reflection of Vapor Grown Single Crystal Platelets of β-Ga_2O_3. *Jpn. J. Appl. Phys.* **1974**, *13*, 1578.
(112) Higashiwaki, M.; Jessen, G. H. Guest Editorial: The Dawn of Gallium Oxide Microelectronics. *Appl. Phys. Lett.* **2018**, *112*, No. 060401.
(113) Tadjer, M. J.; Lyons, J. L.; Nepal, N.; Freitas, J. A., Jr.; Koehler, A. D.; Foster, G. M. Editors' Choice—Review—Theory and Characterization of Doping and Defects in β-Ga_2O_3. *ECS J. Solid State Sci. Technol.* **2019**, *8*, Q3187−Q3194.
(114) Fares, C.; Ren, F.; Lambers, E.; Hays, D. C.; Gila, B. P.; Pearton, S. J. Band Offsets for Atomic Layer Deposited $HfSiO_4$ on $(Al_{0.14}Ga_{0.86})_2O_3$. *ECS J. Solid State Sci. Technol.* **2018**, *7*, P519−P523.
(115) Fares, C.; Ren, F.; Lambers, E.; Hays, D. C.; Gila, B. P.; Pearton, S. J. Valence- and Conduction-Band Offsets for Atomic-Layer-Deposited Al_2O_3 on (010) $(Al_{0.14}Ga_{0.86})_2O_3$. *J. Electron. Mater.* **2019**, *48*, 1568−1573.
(116) Fares, C.; Kneiß, M.; von Wenckstern, H.; Tadjer, M.; Ren, F.; Lambers, E.; Grundmann, M.; Pearton, S. J. Band Alignment of Atomic Layer Deposited SiO_2 and Al_2O_3 on $(Al_xGa_{1-x})_2O_3$ for x = 0.2-0.65. *ECS J. Solid State Sci. Technol.* **2019**, *8*, P351−P356.
(117) Fares, C.; Ren, F.; Hays, D. C.; Gila, B. P.; Pearton, S. J. Effect of Deposition Method on Valence Band Offsets of SiO_2 and Al_2O_3 on $(Al_{0.14}Ga_{0.86})_2O_3$. *ECS J. Solid State Sci. Technol.* **2019**, *8*, Q3001−Q3006.
(118) Wakabayashi, R.; Hattori, M.; Yoshimatsu, K.; Horiba, K.; Kumigashira, H.; Ohtomo, A. Band Alignment at β-$(Al_xGa_{1-x})_2O_3$/ β-Ga_2O_3 (100) Interface Fabricated by Pulsed-Laser Deposition. *Appl. Phys. Lett.* **2018**, *112*, 232103.
(119) Feng, Z.; Feng, Q.; Zhang, J.; Li, X.; Li, F.; Huang, L.; Chen, H. Y.; Lu, H. L.; Hao, Y. Band Alignment of $SiO_2/(Al_xGa_{1-x})_2O_3$ ($0\leq x\leq 0.49$) Determined by X-Ray Photoelectron Spectroscopy. *Appl. Surf. Sci.* **2018**, *434*, 440−444.
(120) Feng, Z.; Feng, Q.; Zhang, J.; Zhang, C.; Zhou, H.; Li, X.; Huang, L.; Xu, L.; Hu, Y.; Zhao, S.; et al. Band Alignments of SiO_2 and HfO_2 Dielectrics with $(Al_xGa_{1-x})_2O_3$ Film ($0\leq x\leq 0.53$) Grown on Ga_2O_3 Buffer Layer on Sapphire. *J. Alloys Compd.* **2018**, *745*, 292−298.
(121) Zhang, F.; Saito, K.; Tanaka, T.; Nishio, M.; Arita, M.; Guo, Q. Wide Bandgap Engineering of $(AlGa)_2O_3$ Films. *Appl. Phys. Lett.* **2014**, *105*, 162107.
(122) Hu, Z.; Feng, Q.; Zhang, J.; Li, F.; Li, X.; Feng, Z.; Zhang, C.; Hao, Y. Optical Properties of $(Al_xGa_{1-x})_2O_3$ on Sapphire. *Superlattices Microstruct.* **2018**, *114*, 82−88.
(123) Kamimura, T.; Sasaki, K.; Hoi Wong, M.; Krishnamurthy, D.; Kuramata, A.; Masui, T.; Yamakoshi, S.; Higashiwaki, M. Band Alignment and Electrical Properties of Al_2O_3/β-Ga_2O_3 Heterojunctions. *Appl. Phys. Lett.* **2014**, *104*, 192104.
(124) Zaffora, A.; Santamaria, M.; Di Franco, F.; Habazaki, H.; Di Quarto, F. Photoelectrochemical Evidence of Nitrogen Incorporation during Anodizing Sputtering-Deposited Al-Ta Alloys. *Phys. Chem. Chem. Phys.* **2016**, *18*, 351−360.
(125) Fogazza, M.; Santamaria, M.; Di Quarto, F.; Garcia-Vergara, S. J.; Molchan, I.; Skeldon, P.; Thompson, G. E.; Habazaki, H. Formation of Anodic Films on Sputtering-Deposited Al−Hf Alloys. *Electrochim. Acta* **2009**, *54*, 1070−1075.
(126) Wei, C. Y.; Shen, B.; Ding, P.; Han, P.; Li, A. D.; Xia, Y. D.; Xu, B.; Yin, J.; Liu, Z. G. Ta_2O_5-TiO_2 Composite Charge-Trapping Dielectric for the Application of the Nonvolatile Memory. *Sci. Rep.* **2017**, *7*, 5988.
(127) Santamaria, M.; Conigliaro, G.; Di Franco, F.; Megna, B.; Di Quarto, F. Electronic Properties of Thermal Oxides on Ti and Their Influence on Impedance and Photoelectrochemical Behavior of TiO_2 Nanotubes. *J. Electrochem. Soc.* **2017**, *164*, C113−C120.
(128) Di Quarto, F.; Di Franco, F.; Miraghaei, S.; Santamaria, M.; La Mantia, F. The Amorphous Semiconductor Schottky Barrier Approach to Study the Electronic Properties of Anodic Films on Ti. *J. Electrochem. Soc.* **2017**, *164*, C516−C525.
(129) Di Quarto, F.; Di Franco, F.; Santamaria, M.; La Mantia, F. Differential Capacitance Measurements on Passive Films. In *Encyclopedia of Interfacial Chemistry: Surface Science and Electrochemistry*; Wandelt, K., Ed.; Elsevier: 2018; pp. 75−92.
(130) Mott, N. F.; Davis, E. A. *Electronic Processes In Non-Crystalline Materials* 2nd ed.; Clarendon Press: Oxford, U.K., 1979.
(131) Franke, E.; Trimble, C. L.; DeVries, M. J.; Woollam, J. A.; Schubert, M.; Frost, F. Dielectric Function of Amorphous Tantalum Oxide from the Far Infrared to the Deep Ultraviolet Spectral Region Measured by Spectroscopic Ellipsometry. *J. Appl. Phys.* **2000**, *88*, 5166−5174.
(132) Aleshina, L. A.; Malinenko, V. P.; Phouphanov, A. D.; Jakovleva, N. M. The Short-Range Order of Anodic Amorphous Oxide Films of Ta and Nb. *J. Non-Cryst. Solids* **1986**, *87*, 350−360.
(133) Maeng, S.; Axe, L.; Tyson, T.; Jiang, A. An Investigation of Structures of Thermal and Anodic Tantalum Oxide Films. *J. Electrochem. Soc.* **2005**, *152*, B60−B64.
(134) Alderman, O. L. G.; Benmore, C. J.; Neuefeind, J.; Coillet, E.; Mermet, A.; Martinez, V.; Tamalonis, A.; Weber, R. Amorphous Tantala and Its Relationship with the Molten State. *Phys. Rev. Mater.* **2018**, *2*, No. 043602.
(135) Robinson, J.; Thompson, G. E.; Shimizu, K. Towards a Structural Model for Anodic Alumina. In *Proceedings of the Seventh International Symposium on Oxide Films on Metals and Alloys*; Hebert, K. R., Thompson, G. E., Eds.; The Electrochemical Society Inc.: 1994; pp *94*, 1−12.
(136) Di Franco, F.; Zampardi, G.; Santamaria, M.; Di Quarto, F.; Habazaki, H. Characterization of the Solid State Properties of Anodic Oxides on Magnetron Sputtered Ta, Nb and Ta-Nb Alloys. *J. Electrochem. Soc.* **2011**, *159*, C33−C39.
(137) Di Quarto, F.; Santamaria, M.; Skeldon, P.; Thompson, G. E. Photocurrent Spectroscopy Study of Passive Films on Hafnium and Hafnium−Tungsten Sputtered Alloys. *Electrochim. Acta* **2003**, *48*, 1143−1156.
(138) Zaffora, A.; Tranchida, G.; Di Franco, F.; Di Quarto, F.; Santamaria, M. Physico-Chemical Characterization of Anodic Oxides on Hf as a Function of the Anodizing Conditions. *J. Electrochem. Soc.* **2016**, *163*, C563−C570.
(139) Zaffora, A.; Di Franco, F.; Di Quarto, F.; Macaluso, R.; Mosca, M.; Habazaki, H.; Santamaria, M. The Effect of Nb Incorporation on the Electronic Properties of Anodic HfO_2. *ECS J. Solid State Sci. Technol.* **2017**, *6*, N25−N31.
(140) Niedermeier, C. A.; Råsander, M.; Rhode, S.; Kachkanov, V.; Zou, B.; Alford, N.; Moram, M. A. Band Gap Bowing in $Ni_xMg_{1-x}O$. *Sci. Rep.* **2016**, *6*, 31230.
(141) Ernst, F.; Pirouz, P.; Heuer, A. H. HRTEM Study of a Cu/Al_2O_3 Interface. *Philos. Mag. A* **1991**, *63*, 259−277.
(142) Aarik, J.; Kasikov, A.; Kirm, M.; Lange, S.; Uustare, T.; Mändar, H. Optical Properties of Crystalline Al_2O_3 Thin Films Grown by Atomic Layer Deposition. In *Proceedings SPIE 5946, Optical Materials and Applications*; Rosental, A., Ed.; SPIE: 2006; Vol. *5946*, p 594601.
(143) Barbos, C.; Blanc-Pelissier, D.; Fave, A.; Botella, C.; Regreny, P.; Grenet, G.; Blanquet, E.; Crisci, A.; Lemiti, M. Al_2O_3 Thin Films Deposited by Thermal Atomic Layer Deposition: Characterization for Photovoltaic Applications. *Thin Solid Films* **2016**, *617*, 108−113.
(144) Shi, C.; Alderman, O. L. G.; Berman, D.; Du, J.; Neuefeind, J.; Tamalonis, A.; Weber, J. K. R.; You, J.; Benmore, C. J. The Structure of Amorphous and Deeply Supercooled Liquid Alumina. *Front. Mater.* **2019**, *6*, 38.
(145) Gaskins, J. T.; Hopkins, P. E.; Merrill, D. R.; Bauers, S. R.; Hadland, E.; Johnson, D. C.; Koh, D.; Yum, J. H.; Banerjee, S.; Nordell, B. J.; et al. Review—Investigation and Review of the

https://dx.doi.org/10.1021/acs.inorgchem.0c02691
Inorg. Chem. 2021, 60, 1419−1435

Thermal, Mechanical, Electrical, Optical, and Structural Properties of Atomic Layer Deposited High-*k* Dielectrics: Beryllium Oxide, Aluminum Oxide, Hafnium Oxide, and Aluminum Nitride. *ECS J. Solid State Sci. Technol.* **2017**, *6*, N189−N208.
(146) Chagarov, E.; Kummel, A. C. Generation of Realistic Amorphous Al_2O_3 And ZrO_2 Samples By Hybrid Classical and First-Principle Molecular Dynamics Simulations. *ECS Trans.* **2008**, *16*, 773−785.
(147) Shi, S.; Qian, S.; Hou, X.; Mu, J.; He, J.; Chou, X. Structural and Optical Properties of Amorphous Al_2O_3 Thin Film Deposited by Atomic Layer Deposition. *Adv. Condens. Matter Phys.* **2018**, *2018*, 7598978.
(148) Balamurugan, C.; Subashini, A.; Chaudhari, G. N.; Subramania, A. Development of Wide Band Gap Sensor Based on $AlNbO_4$ Nanopowder for Ethanol. *J. Alloys Compd.* **2012**, *526*, 110−115.
(149) Soares, M. R. N.; Leite, S.; Nico, C.; Peres, M.; Fernandes, A. J. S.; Graça, M. P. F.; Matos, M.; Monteiro, R.; Monteiro, T.; Costa, F. M. Effect of Processing Method on Physical Properties of Nb_2O_5. *J. Eur. Ceram. Soc.* **2011**, *31*, 501−506.
(150) Mickova, I. Photoelectrochemical Study of Anodically Formed Oxide Films on Niobium Surfaces. *Croat. Chem. Acta* **2010**, *83*, 113−120.
(151) Chun, W. J.; Ishikawa, A.; Fujisawa, H.; Takata, T.; Kondo, J. N.; Hara, M.; Kawai, M.; Matsumoto, Y.; Domen, K. Conduction and Valence Band Positions of Ta_2O_5, TaON, and Ta_3N_5 by UPS and Electrochemical Methods. *J. Phys. Chem. B* **2003**, *107*, 1798−1803.
(152) Di Quarto, F.; Gentile, C.; Piazza, S.; Sunseri, C. A Photoelectrochemical Study on Anodic Tantalum Oxide Films. *Corros. Sci.* **1993**, *35*, 801−808.
(153) Yang, Y.; Kawazoe, Y. Prediction of New Ground-State Crystal Structure of Ta_2O_5. *Phys. Rev. Mater.* **2018**, *2*, No. 034602.
(154) Habazaki, H.; Shimizu, K.; Skeldon, P.; Thompson, G. E.; Wood, G. C. Inter-Relationships between Ionic Transport and Composition in Amorphous Anodic Oxides. *Proc. R. Soc. London, Ser. A* **1997**, *453*, 1593−1609.
(155) Alcalá, G.; Mato, S.; Skeldon, P.; Thompson, G. E.; Bailey, P.; Noakes, T. C. Q.; Habazaki, H.; Shimizu, K. Anodic Film Growth in the Al−Ta Alloy System. *Corros. Sci.* **2003**, *45*, 1803−1813.
(156) Rosales-Sosa, G. A.; Masuno, A.; Higo, Y.; Inoue, H.; Yanaba, Y.; Mizoguchi, T.; Umada, T.; Okamura, K.; Kato, K.; Watanabe, Y. High Elastic Moduli of a $54Al_2O_3$-$46Ta_2O_5$ Glass Fabricated via Containerless Processing. *Sci. Rep.* **2015**, *5*, 15233.
(157) Lima, A. F.; Dantas, J. M.; Lalic, M. V. An *Ab-Initio* Study of Electronic and Optical Properties of Corundum Al_2O_3 Doped with Sc, Y, Zr, and Nb. *J. Appl. Phys.* **2012**, *112*, No. 093709.
(158) Samantaray, C. B.; Sim, H.; Hwang, H. Electronic Structures of Transitional Metal Aluminates as High-k Gate Dielectrics: First Principles Study. *Appl. Surf. Sci.* **2004**, *239*, 101−108.

https://dx.doi.org/10.1021/acs.inorgchem.0c02691
Inorg. Chem. 2021, 60, 1419−1435